

Binary stars in the Galactic thick disc

Robert G. Izzard,¹ Holly Preece,^{1,2} Paula Jofre,^{1,3} Ghina M. Halabi,¹
Thomas Masseron,^{1,4,5} and Christopher A. Tout¹

¹*Institute of Astronomy, Madingley Road, Cambridge, CB3 0HA, United Kingdom.*

²*Armagh Observatory, College Hill, Armagh, BT61 9DG, United Kingdom.*

³*Núcleo de Astronomía, Facultad de Ingeniería, Universidad Diego Portales, Av. Ejército 441, Santiago, Chile.*

⁴*Instituto de Astrofísica de Canarias, E-38205 La Laguna, Tenerife, Spain.*

⁵*Departamento de Astrofísica, Universidad de La Laguna, E-38206 La Laguna, Tenerife, Spain.*

Received ...; Accepted...

ABSTRACT

The combination of asteroseismologically-measured masses with abundances from detailed analyses of stellar atmospheres challenges our fundamental knowledge of stars and our ability to model them. Ancient red-giant stars in the Galactic thick disc are proving to be most troublesome in this regard. They are older than 5 Gyr, a lifetime corresponding to an initial stellar mass of about $1.2 M_{\odot}$. So why do the masses of a sizeable fraction of thick-disc stars exceed $1.3 M_{\odot}$, with some as massive as $2.3 M_{\odot}$? We answer this question by considering duplicity in the thick-disc stellar population using a binary population-nucleosynthesis model. We examine how mass transfer and merging affect the stellar mass distribution and surface abundances of carbon and nitrogen. We show that a few per cent of thick-disc stars can interact in binary star systems and become more massive than $1.3 M_{\odot}$. Of these stars, most are single because they are merged binaries. Some stars more massive than $1.3 M_{\odot}$ form in binaries by wind mass transfer. We compare our results to a sample of the APOKASC data set and find reasonable agreement except in the number of these thick-disc stars more massive than $1.3 M_{\odot}$. This problem is resolved by the use of a logarithmically-flat orbital-period distribution and a large binary fraction.

Stars: binaries: general – Stars: abundances – Galaxy: disc –
Galaxy: abundances – Galaxy: stellar content

1 INTRODUCTION

The stellar evolution of low-mass, those lighter than about $2 M_{\odot}$, single stars is reasonably well understood. Stars form in radiating, collapsing clouds of mostly hydrogen and helium. Compression heats the centre of the clouds until nuclear burning begins in their cores and stars are born. Stars burn hydrogen on the main sequence then ascend the red-giant branch when hydrogen-burning moves into a shell surrounding a helium core (Sandage & Schwarzschild 1952). Subsequently, helium ignites and a stage of core helium-burning, also called the red-clump, follows. Helium subsequently burns in a shell as the star ascends the asymptotic giant branch. Surface mass loss terminates single-star evolution at this stage leaving a carbon-oxygen core which cools into a white dwarf. The main parameters that drive the evolution of single, low-mass stars are the total stellar mass, M , and the metallicity, Z , which is the mass fraction of all elements heavier than hydrogen or helium. The ratio $[\text{Fe}/\text{H}] = \log_{10}(N_{\text{Fe}}/N_{\text{Fe}\odot}) - \log_{10}(N_{\text{H}}/N_{\text{H}\odot})$ is often used as a proxy for the metallicity, where N_i is the surface number density of species i .

The Milky Way contains several populations of low-mass stars that have different metallicities, kinematics and star-formation histories (Bland-Hawthorn & Gerhard 2016). The thin disc is a relatively high-metallicity population in a large disc surround-

ing the centre of the Galaxy. Our Sun is a thin-disc star with $Z = Z_{\odot} \approx 0.014$ or $[\text{Fe}/\text{H}] = 0$ by definition (Asplund et al. 2009; Lodders 2010). At the centre of the Galaxy is the bulge, which contains many old stars at low, solar and higher metallicity. The Galactic halo surrounds the Milky Way out to long distances and contains very old, low-metallicity stars. The remaining stellar population is the Galactic thick disc (Gilmore & Reid 1983). It is thick because its stars have greater spatial velocities. The population is kinetically warmer and more extended out of the Galactic plane, than the thin disc. Generally, thick-disc stars are metal-poor compared to the thin disc but there is substantial overlap in the metallicity distributions of the discs (Navarro et al. 2011). Thick-disc stars are enhanced in alpha elements such as magnesium, as measured through the ratio $[\alpha/\text{Fe}]$. In the solar neighbourhood there are fewer stars in the thick than in the thin disc (Fuhrmann et al. 2017a). Even though the thick disc is a minor stellar component locally, its properties are vital clues to understanding the structure and formation of the Milky Way and galaxies in general (Brook et al. 2012; Bland-Hawthorn & Gerhard 2016; Minchev et al. 2017). The origin of the thick disc remains the subject of debate. Galactic formation models predict few young stars in the thick disc because it formed rapidly soon after the Milky Way was born. The ages of thick-disc stars are thus vital to disentangle the process of galaxy formation and its application to the Milky Way.

The thick disc is at least 5 Gyr old and hence its stars are of low mass (Martig et al. 2016). The main-sequence lifetime of a $Z = 0.008$, $M = 1.15 M_{\odot}$, single star is about 5.2 Gyr, while a

$Z = 0.008$, $M = 0.96 M_{\odot}$, single star lives for 10.0 Gyr (based on Pols et al. 1995’s models). After the main sequence, stars spend about one tenth of the main-sequence lifetime ascending the red giant branch. The initial masses of 5 – 10 Gyr stars lie in a narrow range of mass from about 0.95 to 1.2 M_{\odot} with a small spread owing to a variation in metallicity. In this regard, the thick-disc is similar to a globular cluster in which stars are born roughly at the same time with one metallicity. The properties of thick-disc red giants thus map stellar evolution corresponding to a narrow range of initial parameters.

Recent advances in observational surveys have improved our understanding of the thick-disc stellar population. The *Kepler* mission has allowed the measurement of stellar masses by asteroseismology (e.g. Miglio et al. 2012). Combining stellar masses with follow-up spectroscopy using the Apache Point Observatory Galactic Evolution Experiment (APOGEE), the APOGEE–Kepler Asteroseismic Science Consortium (APOKASC) data of Pinsonneault et al. (2014) provide stellar properties, including surface gravity $\log g$ and chemical abundances such as $[\text{Fe}/\text{H}]$, $[\alpha/\text{Fe}]$ and $[\text{C}/\text{N}]$, which can be compared with stellar evolution models. The $[\text{C}/\text{N}]$ ratio is particularly important because it is expected to be reduced by the mixing of nuclear-processed material to the stellar surface during ascent of the red giant branch. This mixing is due to either first dredge up, caused by a deepening of the stellar convection zone, or other mechanisms such as thermohaline mixing, magnetic mixing or rotational mixing, all of which are known as extra-mixing (e.g. Weiss et al. 2000; Stancliffe et al. 2009; Charbonnel & Lagarde 2010).

Galactic thick disc stars, because of their low mass, are not expected to much change their stellar surface $[\text{C}/\text{N}]$ during ascent of the red-giant branch (Salaris et al. 2015). The convection zone does not mix to great depth, so little nitrogen is mixed to the surface. Thus it is surprising that some stars, selected from the APOKASC sample to be thick-disc members by virtue of their $[\alpha/\text{Fe}]$, have $[\text{C}/\text{N}]$ as low as -0.8 dex (Masseron et al. 2017). Even more strangely, a number of the APOKASC thick-disc stars have masses, measured from asteroseismological scaling relations, in excess of the 1.2–1.3 M_{\odot} upper limit expected from canonical stellar evolution of stars so old. These stars challenge both stellar and Galactic evolution models. Their high masses and alpha enhancements imply that they may have formed in the Galactic centre and subsequently migrated into the thick disc (Chiappini et al. 2015). However, we already know from radial-velocity monitoring that many of the extra-massive thick-disc stars are plausibly multiple systems (Jofré et al. 2016). In this work we test the possibility that these stars originate in multiple stellar systems and their properties arise from binary-star interactions (De Marco & Izzard 2017).

Stars that are more massive than they should be in a population of fixed age are well known to those who study globular clusters. On the main sequence these stars are bluer and brighter. They look younger than stars at the blue end of the main sequence and so they are known as blue stragglers. Blue stragglers form by mass transfer or stellar merging in multiple stellar systems (e.g. Lombardi et al. 2002; Geller & Mathieu 2011). In binary stars, mass transfer either by direct Roche-lobe overflow or wind mass transfer is relatively common (De Marco & Izzard 2017). The increase in mass of a star causes it to look younger than it actually is (Sandage 1953; Tout et al. 1997). There is every reason to believe that such stellar systems exist in the Galactic thick disc (Jofré et al. 2016), however they are more difficult to identify than in stellar clusters because of the lack of a clear turn-off in the Hertzsprung–Russell or colour–magnitude diagram.

The stars in the APOKASC thick-disc sample with mass in

excess of 1.3 M_{\odot} are not blue stragglers. They are red giant stars which may once have been blue stragglers. Indeed, as we show below, a fraction of the extra-massive thick-disc stars were probably once blue stragglers. However mass transfer in a binary system is most likely after the main sequence as the more massive star in the binary ascends the giant branch. This can lead to an increase in mass of a companion star or to common-envelope evolution in which the core of the giant and its companion orbit each other inside a shared stellar envelope (Izzard et al. 2012; Ivanova et al. 2013). Often this leads to envelope ejection but alternatively the stars merge to form a new giant. These stars are quite possibly those that are seen in the APOKASC sample.

In the following we assess the possibility that binary stars make up at least some of the thick-disc stars with mass in excess of 1.3 M_{\odot} . In section 2 we combine detailed stellar evolution models of first dredge up in red giants with a stellar population–nucleosynthesis model to construct populations of red-giant stars suitable for comparison with observations of thick-disc stars. We select a thick disc sample from APOKASC in section 3. In section 4 we examine the properties of our model stars while varying model parameters and initial distributions of masses and periods within reasonable uncertainties. We discuss the implications of our results and suggestions for future modelling in section 5. Our conclusions then follow in section 6.

2 STELLAR MODELLING

We employ two stellar evolution codes to model Galactic thick-disc stars. First, in section 2.1, we calculate a set of detailed stellar evolution models with the Cambridge STARS code to model the nucleosynthesis of carbon and nitrogen from the pre-main sequence to helium ignition in stars of mass 0.8 to 20 M_{\odot} with $10^{-4} \leq Z \leq 0.03$. Second, in sections 2.2–2.4 we describe how we embed our STARS data into our BINARY_C population–nucleosynthesis code. BINARY_C models millions of single and binary stars quickly, so it is ideal to explore the large parameter space associated with binary stars. section 2.5 describes how we model the thick-disc stellar population.

2.1 Detailed stellar modelling with STARS

We construct a grid of 420 detailed stellar models with logarithmically distributed masses, M , in the range 0.8 to 20 M_{\odot} and metallicities $Z = 10^{-4}$, 3×10^{-4} , 0.001, 0.004, 0.02 and 0.03 using the STARS stellar evolution code (Eggleton 1971; Pols et al. 1995). Each metallicity has a corresponding opacity table which accommodates changes in carbon and oxygen compared to the solar mixture (Eldridge & Tout 2004). Initial abundances, by mass fraction, are scaled by $Z/0.02$ with the mix of Anders & Grevesse (1989). The hydrogen abundance $X = 0.76 - 3Z$ and helium abundance $Y = 0.24 + 2Z$. Our initial models start on the pre-main sequence so that any chemical abundance profile set up during that phase is preserved when the star begins central hydrogen burning. The models each have 999 mesh points to minimise numerical diffusion. We set the convective mixing length parameter $\alpha_{\text{MLT}} = 2.0$, the overshoot parameter $\delta_{\text{ov}} = 0.12$ (Schröder et al. 1997) and define the convectively-mixed stellar envelope by $\nabla_r - \nabla_a \geq 0.01$, where ∇_r and ∇_a are the radiative and adiabatic logarithmic gradients of temperature, to avoid numerical noise at its lower boundary. We disable mass loss. Our input models and their parameters, such as

radius and luminosity, are calibrated to those measured for the Sun (Stancliffe & Eldridge 2009).

All these models all pass through the terminal-age main sequence (TAMS) and evolve to helium ignition. First dredge up is modelled in all our stars. The initial time step is chosen to be shorter than 100 yr and is then allowed to vary to keep the mean modulus of the step-to-step variation in the independent variables of the code close to constant. We define the TAMS to be the time when the central hydrogen mass fraction drops below 10^{-5} . Profiles of elemental abundances of hydrogen, helium, carbon, nitrogen and oxygen are sampled at 100 Lagrangian mass co-ordinates $m = m(r)$, equally-spaced between the centre and surface, in each star at the TAMS. These profiles are exported to a lookup table as a function of M , m/M and Z with $0 \leq m/M \leq 1$ and $0 \leq r/R \leq 1$, where R is the stellar radius. In addition, the depth of first dredge up, the post dredge up surface carbon and nitrogen abundances and the surface gravity when the convective envelope is at its deepest are tabulated as a function of M and Z .

2.2 Nucleosynthesis with `BINARY_C`

We use the stellar population nucleosynthesis code `BINARY_C` to model populations of single and binary stars. This is a C port of the binary star evolution (BSE) algorithm developed by Hurley et al. (2002) extended to include nucleosynthesis (Izzard et al. 2004, 2006, 2009). Recent relevant updates include Wind Roche lobe overflow (WRLOF, Abate et al. 2013, 2015), an improved treatment of stellar rotation (de Mink et al. 2013), updated stellar lifetimes (Schneider et al. 2014) and an improved algorithm describing the rate of Roche-lobe overflow (Claeys et al. 2014).

Previous versions of `BINARY_C` treated first dredge up as an instantaneous event on the giant branch. Stellar surface abundances were shifted by amounts tabulated as a function of total stellar mass based on detailed stellar evolution models (Karakas et al. 2002). This approach is insufficiently accurate for this work so we improve the model of first dredge up in `BINARY_C` in stars with $0.8 \leq M/M_{\odot} \leq 20$ by modelling the stellar envelope as a set of shells, as would a detailed stellar evolution code. Each star initially has 200 shells equally spaced in mass.

Initial chemical abundance profiles are linearly interpolated in mass and metallicity based on the TAMS abundance tables of section 2.1. The chemical profile in the interior at the TAMS arises from pre-main sequence (PMS) CN burning and main-sequence pp and CN burning. The CN profile created during the PMS is unchanged during the main sequence except in the stellar core, so the TAMS abundance profile well represents the envelope abundance profile at any stage of the main sequence. In the core the abundance profile changes with time as hydrogen is converted to helium, but it is difficult to expose core material unless there is extreme mass loss so we assume the TAMS abundances apply. Accreted mass is unlikely to mix into the core (section 2.4; also Stancliffe et al. 2007). Wind mass loss is negligible on the main sequence except in the most massive of our stars. Even then, it occurs near the end of the main sequence so the TAMS profile is a reasonable approximation to the true chemical profile.

Hertzsprung gap evolution is too fast for significant nuclear burning so again the TAMS abundances well represent the stellar interior. When the star ascends the giant branch its helium core grows and its convective envelope deepens during first dredge up. This deepening is relevant to our stellar population because we select such giants for comparison with observations. Chemical changes during canonical first dredge up are a result only of mixing, not

nuclear burning, so the TAMS profile is suitable for describing this process (section 2.3).

After helium ignition at the tip of the red giant branch, second and third dredge up in `BINARY_C` are treated as described by Izzard et al. (2006, 2009), although neither process is important to our main conclusions. Our third dredge up efficiency is that of Karakas et al. (2002) without the enhancement required to match the number of carbon-enhanced metal-poor stars (Izzard et al. 2009) or Magellanic-cloud carbon-star luminosity functions (Izzard & Tout 2004).

Our introduction of a shell structure increases the run time of `BINARY_C` from about 0.1 to 1 s per system. While this slows our computations significantly, we take advantage of modern multi-core CPUs, HTCONDOR and the latest `BINARY_C` support tools to offset the extra cost.

2.3 First dredge up in `BINARY_C`

First dredge up is modelled by homogenizing the stellar convective envelope to a depth M_{DUP} given by that calculated in `BINARY_C` based on the algorithm of BSE. We also limit M_{DUP} to the dredge up depth calculated from our `STARS` models as a tabulated function of the mass, M_0 , of the star at the base of the giant branch (the notation of Hurley et al. 2000). This more accurate limit is required to match the `BINARY_C` and `STARS` surface abundances, namely $[C/N] = \log_{10}(N_C/N_{C,\odot}) - (N_N/N_{N,\odot})$, after first dredge up to within 0.1 dex. A comparison between the post-dredge up surface $[C/N]$ in our `BINARY_C` and `STARS` models at various metallicities is shown in Fig. 1. The logarithmic abundances at the stellar surface calculated with the two codes match to within a few hundredths. This is more accurate than the observations to which we compare and hence sufficient for our purposes, especially given that `BINARY_C` remains many orders of magnitude faster than `STARS` yet gives the same result.

2.4 Stellar mass loss and gain in `BINARY_C`

In our single-star models, mass is lost only by stellar winds, the rates of which are described in Appendix A. In binary stars, mass is lost by both stellar winds and Roche-lobe overflow (RLOF). Our default RLOF prescription follows Claeys et al. (2014). This modifies the algorithm of BSE by enhancing the mass-transfer rate so that the stellar radius R remains close to the Roche lobe radius R_L while maintaining numerical stability. This algorithm compares well to detailed binary-evolution models (Wellstein, Langer & Braun 2001) which enforce $R = R_L$ during both fast and slow case-A mass transfer (Schneider et al. 2014).

We model chemical changes that result from mass loss in `BINARY_C` by removing material from successive shells at the surface of the star, so eventually exposing nuclear-processed material at depth. Mass loss is most likely to occur at the end of the main sequence or during subsequent evolution, so our assumption that the abundance profile in the star is that at the TAMS is justified. We assume that first dredge up reaches the same depth as in a star with the same initial mass but without mass loss (see also section 5.9).

Stars gain material either by Roche-lobe overflow or wind mass transfer. Accretion is modelled in `BINARY_C` by adding mass into shells at the surface with the chemical abundance of the surface of the companion star. Each shell is allowed to increase its mass up to 1/200 the initial stellar mass, at which point a new shell is added. If the number of shells exceeds 750, neighbouring shells are merged

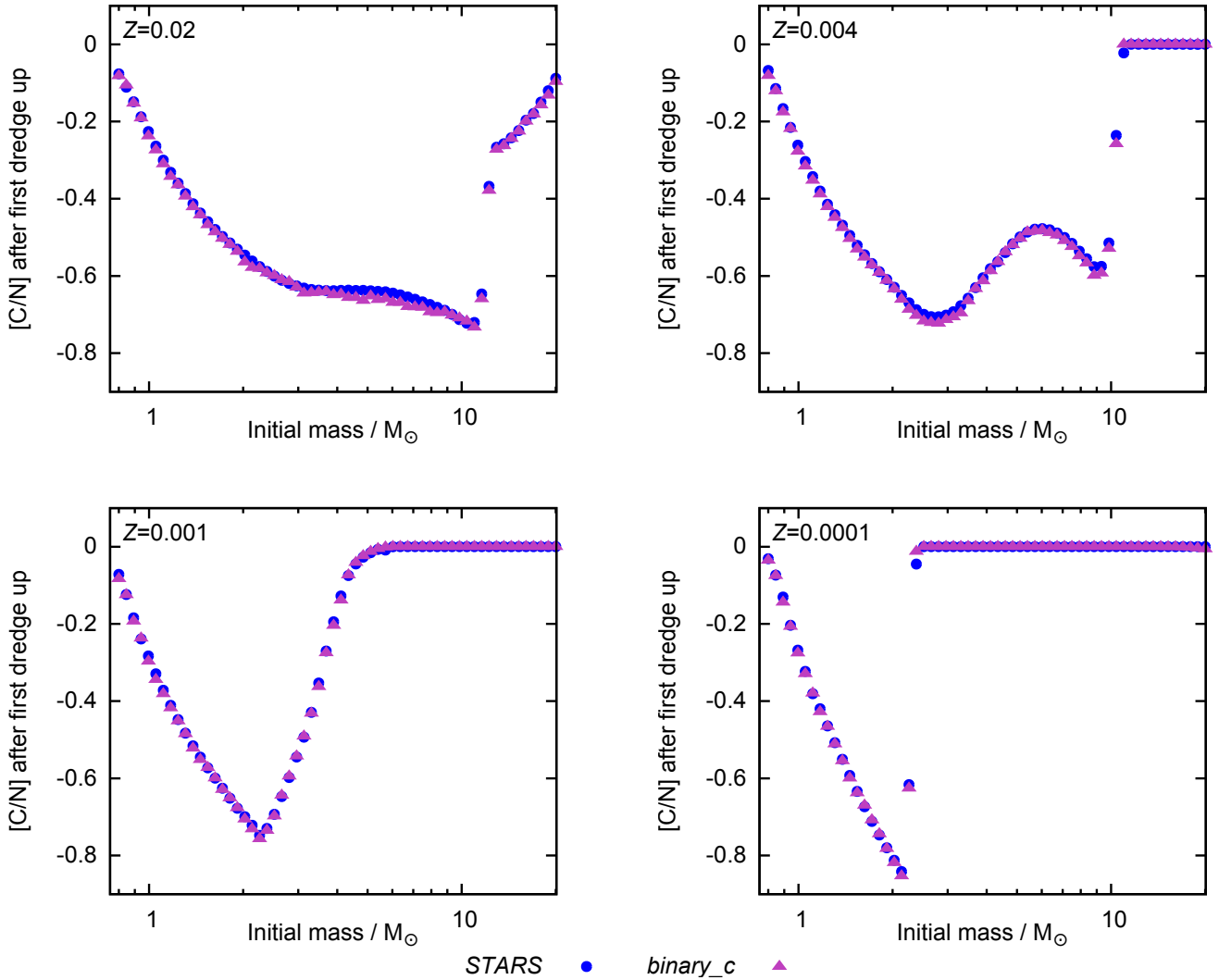


Figure 1. The ratio $[C/N] = \log_{10}(N_C/N_{C,\odot}) - \log_{10}(N_N/N_{N,\odot})$ after first dredge up in our detailed stellar evolution models calculated with the STARS code (blue circles) and our rapid stellar evolution models calculated with BINARY_C (purple triangles). The BINARY_C models each run in less than a second yet reproduce the STARS results to within fractions of a dex over the full mass and metallicity range.

in pairs to halve the number of shells. This limit is chosen to keep code run time short while maintaining accuracy.

Wind mass transfer follows the formalism of [Abate et al. \(2013\)](#) which is based on the smoothed-particle hydrodynamic simulations of [Mohamed & Podsiadlowski \(2007\)](#). This algorithm increases the wind accretion rate relative to the Bondi-Hoyle prescription ([Bondi & Hoyle 1944](#)) in binaries with periods between 10^3 and 10^5 d. In such systems slow winds from red-giant stars are channelled inside the Roche lobe of the accretor so that accretion is very efficient. The numbers of barium, CH and carbon-enhanced metal poor (CEMP) stars are affected by the wind accretion rate. [Abate et al. \(2015\)](#) found that extra mass accretion helps to reconcile the paucity of CEMP stars in our population models to the number observed ([Lee et al. 2014](#)).

When a star accretes, either by RLOF or from a wind, the material it gains may have a greater molecular weight than the stellar envelope below it. If so, thermohaline mixing acts to homogenize the upper part of the envelope until its molecular weight matches the molecular weight of material immediately below the mixed zone.

Our new approach leads to less dilution of accreted material than in our previous study of CEMP stars which assumed full mixing of the star ([Izzard et al. 2009](#)). The detailed models of [Stancliffe et al. \(2007\)](#) show that even a small amount of accretion can cause most of the star to mix. They accrete $0.09 M_{\odot}$ of helium-enhanced material, typical of $2 M_{\odot}$ AGB ejecta with molecular weight 0.657, on to a $0.74 M_{\odot}$, $Z = 10^{-4}$ star with molecular weight 0.593. The resulting $0.83 M_{\odot}$ star mixes by the thermohaline instability to within about $0.1 M_{\odot}$ of its centre in one tenth of the star’s main-sequence life time. We assume thermohaline mixing is instantaneous even though it is expected to act on the stellar thermal time-scale. In all our stars this is much shorter than, typically 10 per cent of, the main-sequence life time ([Denissenkov & Pinsonneault 2008](#) argue that the mixing time-scale should perhaps be much longer than the star’s thermal time-scale). We do not include gravitational settling, radiative levitation or rotational mixing which could also alter the surface abundances of old stars ([Matrozi & Stancliffe 2016, 2017](#)).

When two dwarf stars merge their combined envelope is sorted by molecular weight. This simulates the results of detailed stellar

evolution models of low-mass merged stars by the use of molecular weight as a proxy for entropy (Gaburov et al. 2008; Sills & Glebbeek 2010; Ivanova et al. 2013). When a binary star enters a common envelope phase both stellar envelopes are homogenized in the process under the assumption that the orbital energy and angular momentum deposited in the common envelope mixes it completely prior to ejection or merging. The relatively compact cores in the common envelope are not mixed with the envelope.

2.5 Stellar populations with `BINARY_C`

Our stellar population models each contain 10^4 single stars (model sets *S*n**) or 100^3 binary stars (model sets *B*n**), evolved up to 13.7 Gyr. Model sets X and Y are 50 : 50 mixtures of model sets S1 and B1, i.e. they have an initial binary fraction similar to that of solar-neighbourhood stars of mass around $1 M_{\odot}$ (Raghavan et al. 2010). Primary masses, M_1 , are distributed between 0.1 and $6 M_{\odot}$ according to the initial mass function of Kroupa, Tout & Gilmore (1993). Secondary masses follow a flat distribution in the mass ratio $q = M_2/M_1$ such that $0.1 M_{\odot}/M_1 \leq q \leq 1$. Orbital parameters are distributed either as a hybrid orbital-period distribution (Appendix B1) which interpolates between the log-normal distribution of solar-neighbourhood G/K dwarfs at around $1 M_{\odot}$ (Duquennoy & Mayor 1991) and a distribution appropriate to O-type stars at high mass (Sana et al. 2012), or orbital separations, a , are distributed according to a flat- $\ln a$ distribution between 3 and $10^4 R_{\odot}$ (Appendix B2).

Our stars have a default metallicity $Z = 0.008$ (section 3 and Fig. 2) but we also evolve populations with $Z = 10^{-4}$, 0.001 and 0.02. The chemical composition of our stars is a solar-scaled mixture based on Anders & Grevesse (1989) with $[C/Fe]$ enhanced by +0.2 dex to match the chemical evolution of the thick disc (Bensby & Feltzing 2006; Masseron & Gilmore 2015). We do not enhance the α -element abundances because our `BINARY_C` stellar evolution models assume solar-scaled abundances.

Our single-star evolution defaults to the `SSE` and `BSE` standard models of Hurley et al. (2000) and Hurley et al. (2002) respectively. Nucleosynthesis is described in section 2.2. Our binary-star evolution model sets include the following physics as defined in Table 1.

- Wind-Roche-lobe overflow (WRLOF) follows the description of Abate et al. (2013) using their Eqs. 5 or 9, based on the detailed hydrodynamic models of Mohamed & Podsiadlowski (2007), or the Bondi-Hoyle prescription described in Hurley et al. (2002).

- Common envelopes are treated according to the energy-balance algorithm described by Hurley et al. (2002) with parameters $\alpha_{CE} = 0.2$ and λ_{CE} fitted to the models of Dewi & Tauris (2000). We also test $\alpha_{CE} = 0.5$ and 1.0.

- The Companion Reinforced Attrition Process (CRAP) of Tout & Eggleton (1988) is applied with a parameter $B_C = 0$ (i.e. disabled by default, as by Hurley et al. 2002), 10^3 or 10^4 . This process enhances the stellar wind mass loss rate, \dot{M}_{wind} , because of the tidal influence of a companion star according to

$$\dot{M}_{wind} = \dot{M}_{wind}(B_C = 0) \times \left(1 + B_C \max \left[\frac{1}{2}, \frac{R}{R_L} \right]^6 \right) \quad (1)$$

where R and R_L are the stellar radius and Roche radius, respectively, and $\dot{M}_{wind}(B_C = 0)$ is the mass-loss rate in the absence of CRAP.

- Material lost from the system during non-conservative RLOF carries the specific angular momentum of the accretor (our default model, $\gamma_{RLOF} = -2$), the donor ($\gamma_{RLOF} = -1$), or a frac-

tion $\gamma_{RLOF} \geq 0$ of the specific orbital angular momentum, where $\gamma_{RLOF} = 0, 1$ or 2.

- RLOF is based on the formalism of Claeys et al. (2014) which defines the mass-transfer rate as a steep function of the ratio R/R_L . Alternatives include the original `BSE` prescription (Hurley et al. 2002) and the adaptive-RLOF of Schneider et al. (2014) who compute the mass-transfer rate such that $R = R_L$.

- Tides are based on Hut (1981) as prescribed by Hurley et al. (2002) with time-scales from Zahn (1977). The parameter E_2 is as fitted by Siess et al. (2013).

We form stars at a constant rate between 5 and 10 Gyr ago such that our thick-disc model stars have masses between about 0.95 and $1.3 M_{\odot}$ to match the bulk population in our thick-disc observational sample (section 3). Either star in a binary can contribute to stellar number counts and if both stars concurrently satisfy our thick-disc criteria then both are counted separately. The number of such systems is very small.

We also make model sets containing stars with ages between 8 and 13 Gyr which are more typical for the thick disc (Feltzing & Bensby 2009; Haywood et al. 2013). We also consider, in model set Y, a limited range of surface gravity to match selection effects of the APOKASC sample.

We count stars with a radial velocity amplitude exceeding 1 km s^{-1} as binaries. This limit is comparable to that in the observations to which we compare (section 3). We take into account the fact that binary star systems are randomly inclined when calculating our modelled number counts (Appendix C). We also count blue stragglers which are defined as main-sequence stars which have accreted mass and are older than the main-sequence lifetime appropriate to their mass (cf. Hurley et al. 2001).

3 OUR OBSERVATIONAL SAMPLE

We extract a sample of thick-disc stars from APOKASC (Pinsonneault et al. 2014). Abundance data, i.e. $[Fe/H]$, $[C/N]$ and $[\alpha/Fe]$, are from the APOGEE data release 12 Holtzman et al. (2015). Asteroseismological masses and stellar parameters (T_{eff} , $\log g$) are from Pinsonneault et al. (2014). Nuclear-burning stage identifications, such as hydrogen-shell burning or core-helium burning (red clump), are from Elsworth et al. (2017). Most of these stars are relatively unevolved red giants ($\log_{10}[g/\text{cm}^2\text{s}^{-1}] \gtrsim 2.1$) or are helium-burning in the red clump.

From APOKASC we have 1989 giant stars. We select thick-disc stars based on the abundance of α elements, $[\alpha/Fe]$, such that thick-disc stars satisfy,

$$[\alpha/Fe] > -0.06 \times [Fe/H] + 0.1. \quad (2)$$

This leaves us with 345 stars. Of these, 75 (21 per cent), 47 (14 per cent) and 31 (9 per cent) have masses exceeding 1.2, 1.3 and $1.4 M_{\odot}$ respectively (Fig. 2a). If we select, in addition to Eq. (2), only stars with $[Fe/H] < -0.2$, the fraction of the remaining 189 stars with mass exceeding 1.2, 1.3 and $1.4 M_{\odot}$ is 17 per cent, 11 per cent and 6 per cent respectively. There is a significant population of thick-disc stars in excess of $1.3 M_{\odot}$ regardless of metallicity. Mass estimates have a typical associated error of $0.15 M_{\odot}$ although some stars have mass uncertainties of $0.3 M_{\odot}$ (Miglio et al. 2012; Brogaard et al. 2016; Davies & Miglio 2016; Miglio et al. 2016).

The metallicity distribution of our thick-disc selection is shown in Fig. 2b. The distribution peaks at a metallicity of about 0.008 assuming that abundances are solar-scaled and that $[Fe/H] = 0$ corresponds to $Z_{\odot} = 0.014$. We thus use $Z = 0.008$ in our population

Model set	Single/binary	Metallicity	Parameters
S1	Single	0.008	As SSE/BSE (see text).
S2	Single	0.0001	As S1 with $Z = 0.0001$
S3	Single	0.001	As S1 with $Z = 0.001$
S4	Single	0.02	As S1 with $Z = 0.02$
S5	Single	0.008	As S1 with star formation between 8 and 13 Gyr
S6	Single	0.008	As S1 with $2 \leq \log_{10}(g/\text{cm}^2\text{s}^{-1}) \leq 3$
B1	Binary	0.008	$Z = 0.008, \alpha_{\text{CE}} = 0.2, B_{\text{C}} = 0, q_{\text{crit}} = 1.6, \gamma_{\text{RLOF}} = -2$, RLOF Claeys (2014), WRLOF Abate (2013) eq. (5), hybrid initial-period distribution
B2	Binary	0.0001	As B1 with $Z = 0.0001$
B3	Binary	0.001	As B1 with $Z = 0.001$
B4	Binary	0.02	As B1 with $Z = 0.02$
B5	Binary	0.008	As B1 with $q_{\text{crit}} = 1.8$
B6	Binary	0.008	As B1 with $q_{\text{crit}} = 3$
B7	Binary	0.008	As B1 with $\alpha_{\text{CE}} = 0.5$
B8	Binary	0.008	As B1 with $\alpha_{\text{CE}} = 1$
B9	Binary	0.008	As B1 with no WRLOF
B10	Binary	0.008	As B1 with WRLOF Abate 2013 eq. (9)
B11	Binary	0.008	As B1 with BSE RLOF
B12	Binary	0.008	As B1 with adaptive RLOF of Schneider (2014)
B13	Binary	0.008	As B1 with $B_{\text{C}} = 10^3$
B14	Binary	0.008	As B1 with $B_{\text{C}} = 10^4$
B15	Binary	0.008	As B1 with $\gamma_{\text{RLOF}} = -1$ (from donor)
B16	Binary	0.008	As B1 with $\gamma_{\text{RLOF}} = 0$
B17	Binary	0.008	As B1 with $\gamma_{\text{RLOF}} = 1$
B18	Binary	0.008	As B1 with $\gamma_{\text{RLOF}} = 2$
B19	Binary	0.008	As B1 with logarithmically-flat initial-separation distribution
B20	Binary	0.008	As B1 with star formation between 8 and 13 Gyr
B21	Binary	0.008	As B1 with $2 \leq \log_{10}(g/\text{cm}^2\text{s}^{-1}) \leq 3$
X	Mixed	0.008	$\frac{1}{2}$ S1 + $\frac{1}{2}$ B1
Y	Mixed	0.008	$\frac{1}{2}$ S6 + $\frac{1}{2}$ B21, i.e. as S6 with $2 \leq \log_{10}(g/\text{cm}^2\text{s}^{-1}) \leq 3$

Table 1. Parameters of our BINARY_C stellar-population model sets. Column one labels the model set, column two shows the multiplicity, column three the metallicity and column four any other parameters which are changed. S1 and B1 are our default model sets, X best represents the Galactic thick disc and Y our APOKASC thick-disc sample.

models. The tail of the distribution, with metallicities in excess of Z_{\odot} , may contain thin-disc stars which contaminate our thick-disc sample (cf. Navarro et al. 2011). Eq. (2) demands that $[\alpha/\text{Fe}] \lesssim 0.1$ when $[\text{Fe}/\text{H}] = 0.2$. At this and higher metallicity, the measurement error on $[\alpha/\text{Fe}]$ is similar to the lower limit of Eq. (2) and hence $[\alpha/\text{Fe}]$ cannot be used reliably to determine thick- or thin-disc membership. Despite this uncertainty, most of our stars with mass in excess of $1.3 M_{\odot}$ have $[\text{Fe}/\text{H}] < -0.2$ can be attributed to the thick-disc.

4 RESULTS

In this section we compare our thick-disc stellar population models to our thick-disc stellar sample extracted from APOKASC. We focus on $[\text{C}/\text{N}]$ vs. mass, core-mass or $\log g$. In the figures that follow, the number of stars in each bin is represented by the depth of shading which is proportional to the log of the number of stars in each bin. The colour gives the binary fraction with red single and blue binary. We provide the number of stars in excess of $1.3 M_{\odot}$ and their properties because such stars can only form in our models by binary-star interaction. Our model set data are in Table 2.

4.1 Single stars

Our single-star, $Z = 0.008$ thick-disc population is compared with the APOKASC observational sample in the left column of Fig. 3.

The peak of the distribution of $[\text{C}/\text{N}]$ vs. mass (Fig. 3 S1a), at around $M = 1.0 \pm 0.1 M_{\odot}$ and $[\text{C}/\text{N}] = 0.0 \pm 0.2$, and the spread of masses in our single-star models, from about $0.8 M_{\odot}$ to $1.3 M_{\odot}$ agrees well with the bulk of the observed stars. This agreement is by design because we choose our stellar ages, 5 to 10 Gyr, to match the APOKASC asteroseismological masses (section 3). We also boost our initial $[\text{C}/\text{N}]$ by +0.2 dex to mimic chemical evolution in the thick disc. Importantly, none of our single-star models has a mass exceeding $1.3 M_{\odot}$.

The distribution of core masses is as expected from single-star evolution (Fig. 3 S1b). Red giants contribute to the peak at $0.2 - 0.3 M_{\odot}$ because this is when their evolution, and hence core mass growth rate, is slowest. Core helium-burning and asymptotic giant stars give the peak at around $0.5 M_{\odot}$.

Our model giants are in all stages of post-main sequence, giant-star evolution, Hertzsprung gap, giant branch, core helium burning (red clump) and the asymptotic giant branch so these stars have surface gravities, $\log_{10}(g/\text{cm}^2\text{s}^{-1})$, from +4, typical of the main-sequence turn-off, to 0, typical of asymptotic giant branch (AGB) stars (Fig. 3 S1c). Model sets S6, B6 and Y select only stars with $+2 \leq \log_{10}(g/\text{cm}^2\text{s}^{-1}) \leq +3$ to better match APOKASC and are discussed in section 4.3 below.

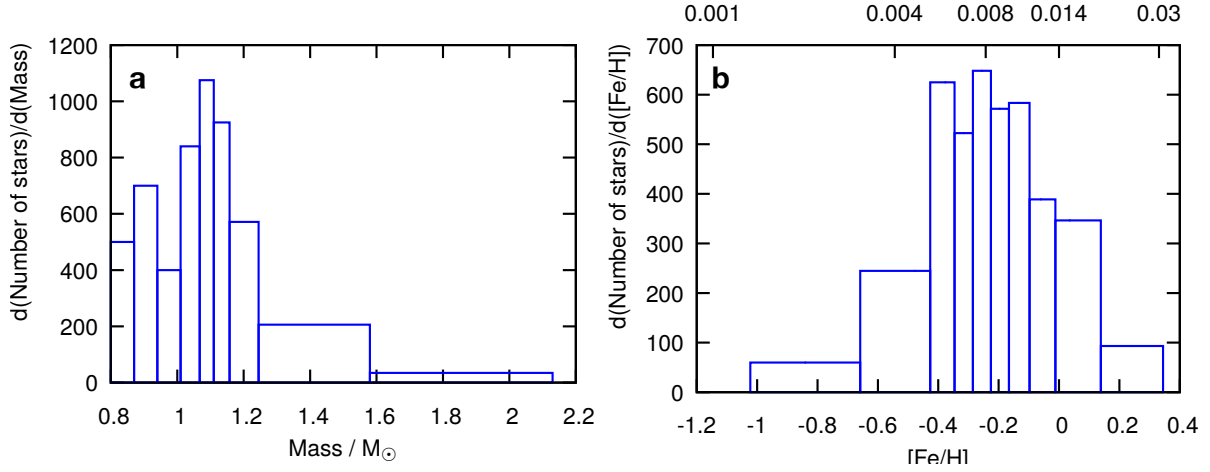


Figure 2. Mass (left, **a**) and metallicity (right, **b**) distributions in our selection of thick-disc giant stars from APOKASC. In **b** the lower abscissa shows $[\text{Fe}/\text{H}] = \log_{10}(N_{\text{Fe}}/N_{\text{Fe},\odot}) - \log_{10}(N_{\text{H}}/N_{\text{H},\odot})$ while the upper shows $Z \approx Z_{\odot} 10^{[\text{Fe}/\text{H}]}$ where $Z_{\odot} = 0.014$ and N_i are number densities of species i at the stellar surface.

Model	Of all giants $M > 1.3 M_{\odot}$	Of giants with $M > 1.3 M_{\odot}$						
		$[\text{C}/\text{N}] \geq 0$	$[\text{C}/\text{N}] < 0$	$[\text{C}/\text{N}] > 0.5$	Single	Binary	was BSS	never BSS
S1	0	0	0	0	0	0	0	0
S2	0	0	0	0	0	0	0	0
S3	0	0	0	0	0	0	0	0
S4	0	0	0	0	0	0	0	0
S5	0	0	0	0	0	0	0	0
S6	0	0	0	0	0	0	0	0
B1	1.7%	0.88%	99%	0.030%	88%	12%	16%	84%
B2	1.0%	5.1%	95%	0.65%	99%	1.0%	11%	90%
B3	1.2%	1.7%	98%	0.70%	99%	0.68%	9.1%	91%
B4	2.8%	0.79%	99%	0	68%	32%	34%	66%
B5	1.7%	0.89%	99%	0.030%	88%	12%	16%	84%
B6	1.7%	0.90%	99%	0.030%	88%	12%	15%	85%
B7	1.3%	0.84%	99%	0.030%	84%	16%	21%	79%
B8	0.93%	0.65%	99%	0.020%	79%	21%	27%	73%
B9	1.5%	0.96%	99%	0.030%	99%	0.67%	6.9%	93%
B10	1.5%	0.98%	99%	0.030%	95%	4.7%	10%	90%
B11	1.8%	0.83%	99%	0.030%	89%	11%	15%	85%
B12	1.7%	1.1%	99%	0.040%	88%	12%	16%	84%
B13	1.5%	0.36%	100%	0.010%	81%	19%	23%	77%
B14	1.0%	0.14%	100%	0.010%	65%	35%	38%	62%
B15	1.7%	0.88%	99%	0.030%	88%	12%	16%	84%
B16	1.7%	0.88%	99%	0.030%	88%	12%	16%	84%
B17	1.7%	0.88%	99%	0.030%	88%	12%	16%	84%
B18	1.7%	0.88%	99%	0.030%	88%	12%	16%	84%
B19	11%	0.45%	100%	0.010%	97%	2.9%	12%	88%
B20	0.81%	0.68%	99%	0.070%	99%	1.4%	8.7%	91%
B21	3.0%	0.41%	100%	0	93%	7.5%	11%	89%
X	0.95%	0.88%	99%	0.030%	88%	12%	16%	84%
Y	1.7%	0.41%	100%	0	93%	7.5%	11%	89%

Table 2. Results of our simulations of thick-disc giant populations of single and binary stars. The physical parameters corresponding to the datasets specified in column one are defined in Table 1. Column two shows the fraction of giant stars in a population which have masses above $1.3 M_{\odot}$. The remaining columns show fractions of these stars with $M > 1.3 M_{\odot}$ with various properties: abundance as measured by $[\text{C}/\text{N}]$, the fractions which would be observed as single and binary, and the fractions that were and were not a blue straggler star (BSS) prior to ascent of the giant branch, respectively.

4.2 Binary stars

In the right panels of Fig. 3 we show the results of repeating the above analysis with model set B1, a population of, initially, only binary stars. The bulk of our APOKASC sample stars coincide with the bulk of our model B1 stars, just as with our single-star model

set S1 (section 4.1). The predicted observed binary fraction in the bulk of the stars, around $M = 1.0 \pm 0.1 M_{\odot}$ and $[\text{C}/\text{N}] = 0.0 \pm 0.2$, is about 65 per cent. While all stars in this model set B1 are born binary, evolution and inclination reduce the observed binary fraction to less than 100 per cent. Our binary stars have their $[\text{C}/\text{N}]$ boosted by $+0.2$ dex identically to our single stars.

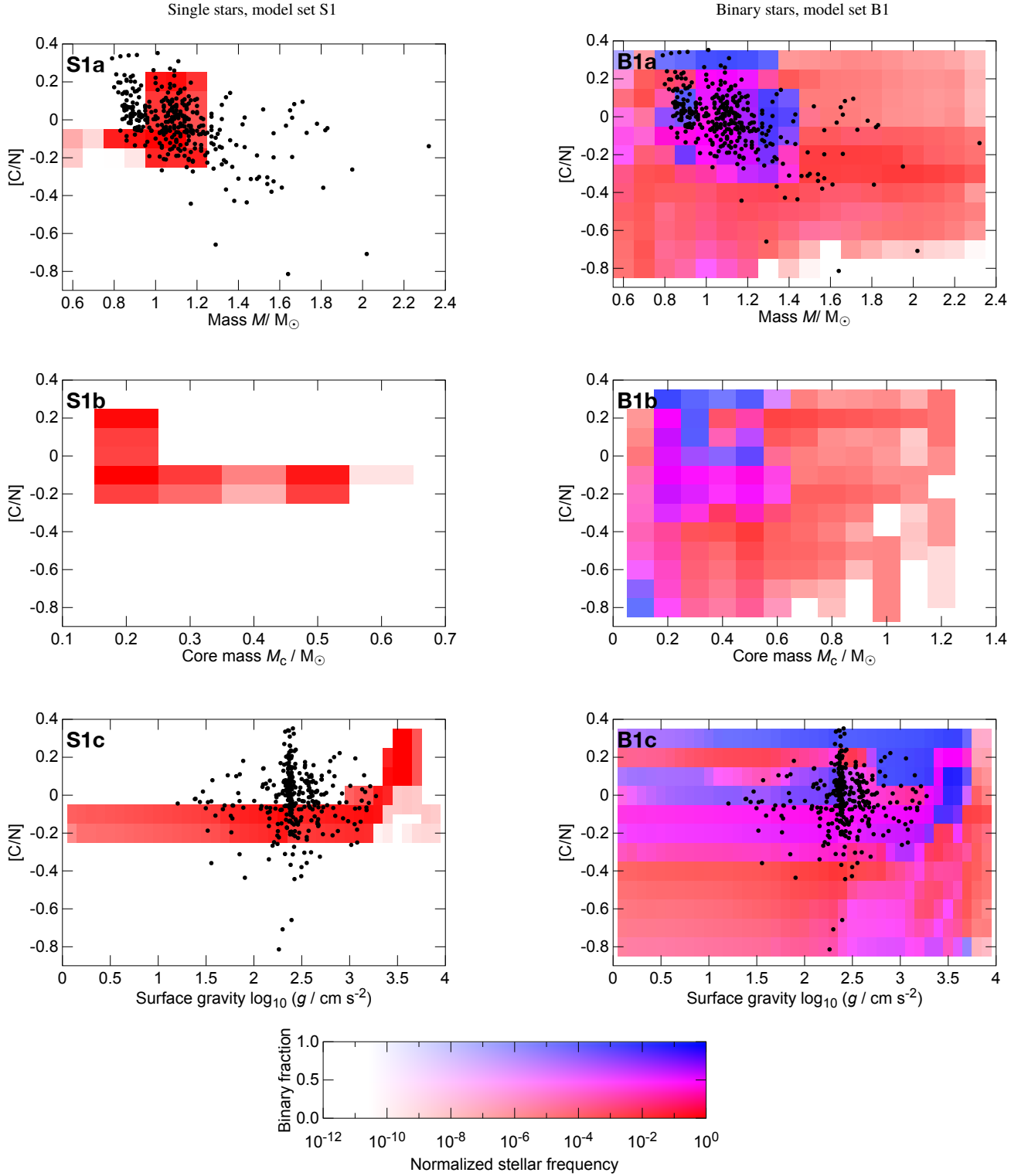


Figure 3. Properties of our thick-disc stellar population models sets S1 (all single stars) and B1 (all binary stars) of the thick disc made with `BINARY_C` vs. our APOKASC thick-disc stellar sample (black points). The top row (a) shows $[C/N]$ vs. mass, middle row (b) shows $[C/N]$ vs. core mass and the bottom row (c) shows $[C/N]$ vs. $\log g$. The depth of shading represents the logarithm of the number of stars in each bin relative to the maximum in each panel. The colour is the binary fraction: single stars are red while binary stars are blue. We show $-0.9 \leq [C/N] \leq 0.4$ to match the range of the APOKASC data, excluding its one star with $[C/N] \approx +1$.

Outside the bulk population, the products of binary evolution are scattered throughout the M vs $[C/N]$ plane. In particular, stars with masses in excess of $1.3 M_{\odot}$, which can only be made in binaries, make up 1.7 per cent of the giants. Most of these, 88 per cent, and almost all stars with masses in excess of $1.5 M_{\odot}$, are single, meaning they are merged binaries. Of these merged stars, 16 per cent are blue-stragglers during the main sequence. The rest, 84 per cent, merge as giants during common envelope evolution.

Mass accretion drives stars to the right in Fig. 3 B1a, while mixing tends to drive stars downwards by decreasing $[C/N]$. The mixing is caused either by common envelope evolution or subsequent first dredge up in the star. We assume that merged stars have first dredge up equally as deep as in a single star of the same mass. This is likely a simplification but our model stars still cover a similar parameter space to the APOKASC sample (see also section 5.9).

We also see a population of stars which gain mass by wind accretion and remain observable as binaries. These accrete up to $0.3 M_{\odot}$ from the wind of their companion while on the main sequence (Abate et al. 2013) and remain polluted as they ascend the giant branch. As for the merged stars, after accretion these stars subsequently reduce their $[C/N]$ by first dredge up so $0.3 < [C/N] < -0.5$. Stars that accrete from an AGB companion are often rich in carbon with $[C/N] \gtrsim 0.2$. These would likely be rejected by APOKASC and are discussed further in section 4.4.

The distributions of $[C/N]$ vs. core mass (Fig. 3 B1b) and $[C/N]$ vs. $\log_{10}(g/\text{cm}^2\text{s}^{-1})$ (Fig. 3 B1c) peak similarly to the single stars of model set S1, but are smeared out by binary interactions. Stars with core masses above $0.6 M_{\odot}$, and those with $[C/N] < -0.4$, are almost all merged binaries. This prediction is being tested by observations, the first results of which are reported in Jofré et al. (2016).

4.3 A thick-disc stellar population

In Fig. 4 we show two populations which contain a mix of initially single and initially binary stars. The first, model set X, is a 50:50 mix of model sets S1 and B1, our default single- and binary-star populations. A 50 per cent binary fraction represents stars of around 1 to $1.2 M_{\odot}$ in the solar neighbourhood (Raghavan et al. 2010) and we assume this also represents the thick disc, as Yuan et al. (2015) suggests. Model set X is thus the population of red giants in the thick disc with no selection criterion except our 1 km s^{-1} radial velocity cut (section 2.5). Model set Y is identical to set X except that it contains only stars with $2 \leq \log_{10}(g/\text{cm}^2\text{s}^{-1}) \leq 3$ to better match the APOKASC sample.

The fractions of stars more massive than $1.3 M_{\odot}$ are 0.95 per cent and 1.7 per cent in model sets X and Y, with binary fractions 12 per cent and 7.5 per cent, respectively. In this respect the data sets are quite similar but they differ because the $\log g$ restriction in model set Y preferentially selects red clump (helium burning) stars. These have core masses around the helium ignition core mass, $0.48 M_{\odot}$ at $Z = 0.008$, so model set Y has an excess of stars with this core mass (section 5.5).

The distributions of binary properties are also similar in model sets X and Y (Table 2). In the following sections we discuss the thick-disc giants in general, our model set X, rather than the APOKASC-specific model set Y. Our conclusions are essentially the same except for the core-mass distribution. Model set X, without the $\log g$ restriction, is likely more applicable to future surveys.

4.4 Extended parameter space

Most stars in our thick-disc APOKASC selection have $-0.8 \leq [C/N] \leq 0.4$ and one has $[C/N] = +1.0$. Fig. 5 shows our model set X predictions over the full range of $[C/N]$ against mass. Almost all our model stars with mass exceeding $1.5 M_{\odot}$ are single, merged binaries. While most of these are first giant branch stars, with $-1 \lesssim [C/N] \lesssim 0$ corresponding to first dredge up appropriate to their mass, we predict a number of stars with significant carbon excess, $[C/N] > 0$ (0.88 per cent of all giants in model set X), some of which have mass in excess of $2 M_{\odot}$.

Many of these carbon-rich stars and all those with $M > 1.5 M_{\odot}$ are single, asymptotic giants (AGB stars). They accrete sufficient mass to exceed the minimum mass for third dredge up (around $1.2 M_{\odot}$, Izzard & Tout 2004) and hence enhance their surface carbon abundance. The one APOKASC star with $[C/N] = +1$ and $M \approx 1 M_{\odot}$ could be a thermally-pulsing AGB star that was previously more massive but has since lost material in its stellar wind. Few of these stars are expected to be seen in APOKASC because the thermally-pulsing AGB (TPAGB) phase is short in duration relative to both the giant branch and red clump. However, they should be anomalously luminous compared to first giant branch stars. *Gaia* distances may help here.

Related to this population are the binary stars with mass around $1.1 M_{\odot}$ which also have enhanced surface carbon. These are the equivalent of barium, CH and CEMP stars. Carbon-rich material is accreted from a more massive asymptotic giant companion while these stars are on the main sequence. Despite thermohaline dilution and the effects of first dredge up, the stars remain carbon rich as they ascend the giant branch. In model set B2, with $Z = 10^{-4}$, 0.65 per cent of stars have $[C/N] > 0.5$, a similar fraction to the approximately 1 per cent of halo stars which are CH stars and the 1 per cent of G/K giants which are barium stars (Jorissen et al. 1998). We discuss the implications of wind mass transfer further in section 5.6.

The binary stars in model set X with masses below $0.6 M_{\odot}$ and decreased $[C/N]$, so enhanced surface nitrogen, are stripped red giants which are similar to low-mass Algol systems. Mass transfer exposes CN-cycled material in their cores. Because of their low mass, reduced luminosity and anomalous $[C/N]$, these stars are likely not selected in APOKASC. These Algols number 0.1 – 0.3 per cent of all giant stars in all our data sets except B19 with 1.9 per cent which is enhanced because of the logarithmically-flat initial-separation distribution (Appendix B2). If the number of Algol systems could be reliably measured as a fraction of the number of red giants, it would provide a powerful diagnostic of the initial binary period distribution. These stars may weak G-band stars which are carbon poor and nitrogen rich (Adamczak & Lambert 2013; Palacios et al. 2016) for which monitoring of duplicity is rather incomplete.

4.5 Variation of parameters

Our main conclusions are relatively robust to uncertainties in our model parameters. The fraction of giants with mass in excess of $1.3 M_{\odot}$ is 0.8 to 3 per cent in all our binary-star model sets except B19. It is 1.7 per cent in our initially 100 per cent binary population (model set B1), 0.95 per cent in our 50:50 mix of single and binary stars (model set X), and is 1.7 per cent in our $\log g$ -selected model set (Y) which should match the APOKASC sample. The finer details, such as binary fraction among the stars more massive than $1.3 M_{\odot}$ and the number of carbon-rich stars, vary somewhat from set to set.

Model sets B5 and B6 test whether changing the critical mass

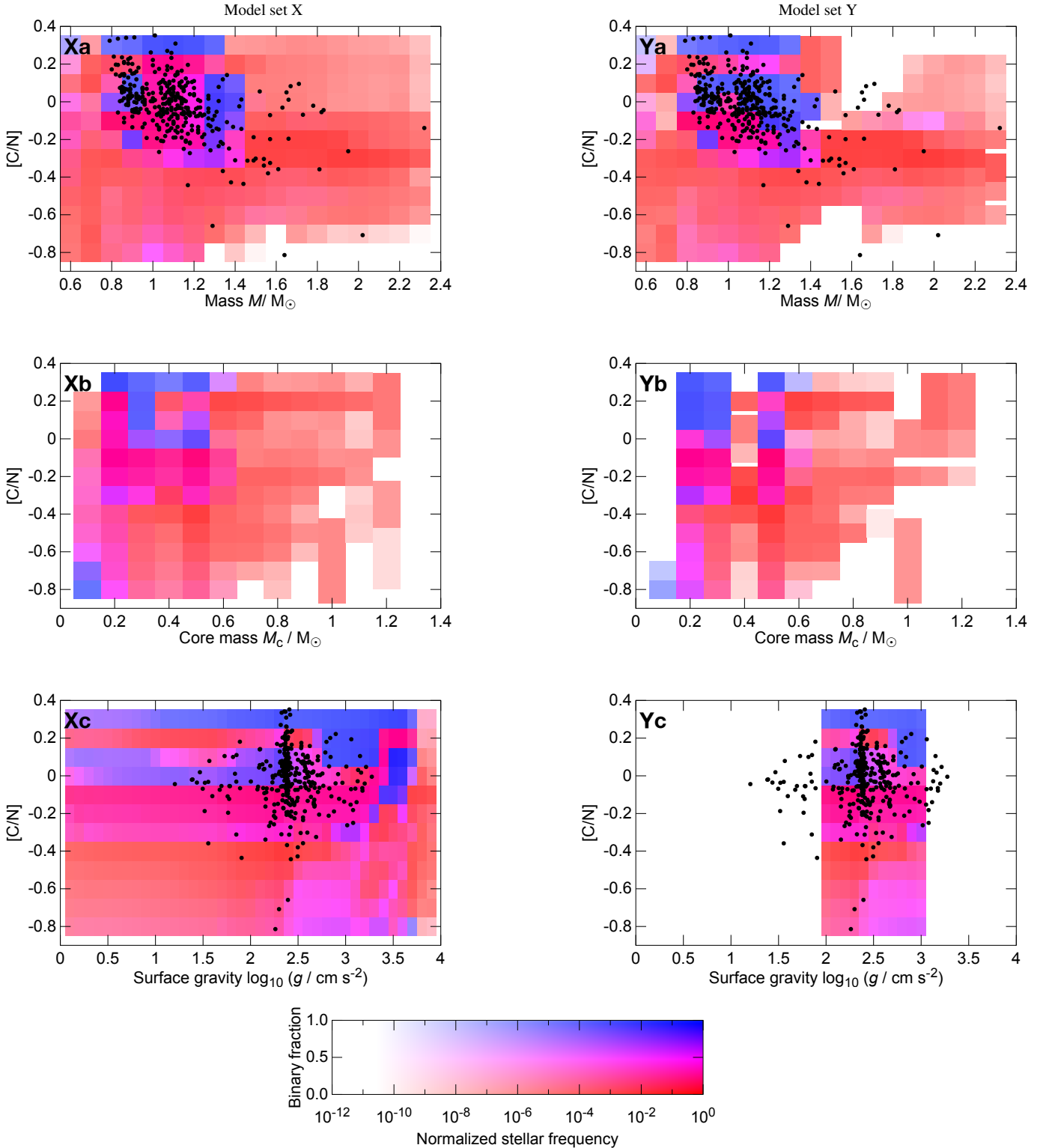


Figure 4. As Fig. 3 with populations of 50 per cent single and 50 per cent binary stars. In the left column $\log g$ is unconstrained (model set X) while in the right column we select only stars with $2 \leq \log_{10}(g / \text{cm}^2 \text{s}^{-1}) \leq 3$ (model set Y) to match our thick-disc sample from APOKASC.

ratio for mass transfer on the main sequence is important to our results. It is not. Varying the parameter only slightly changes the number of blue straggler stars. Model sets B7 and B8 test variations of the common-envelope ejection efficiency parameter with $\alpha_{\text{CE}} = 0.5$ and 1 respectively. Increasing the efficiency of common-

envelope ejection reduces the number of merged stars but, even with $\alpha_{\text{CE}} = 1$ (model set B8), 79 per cent of stars more massive than $1.3 M_{\odot}$ form by merging inside a common-envelope.

Model set B9, with no wind-RLOF, has only 0.67 per cent giants more massive than $1.3 M_{\odot}$ that are binary. Canonical Bondi-

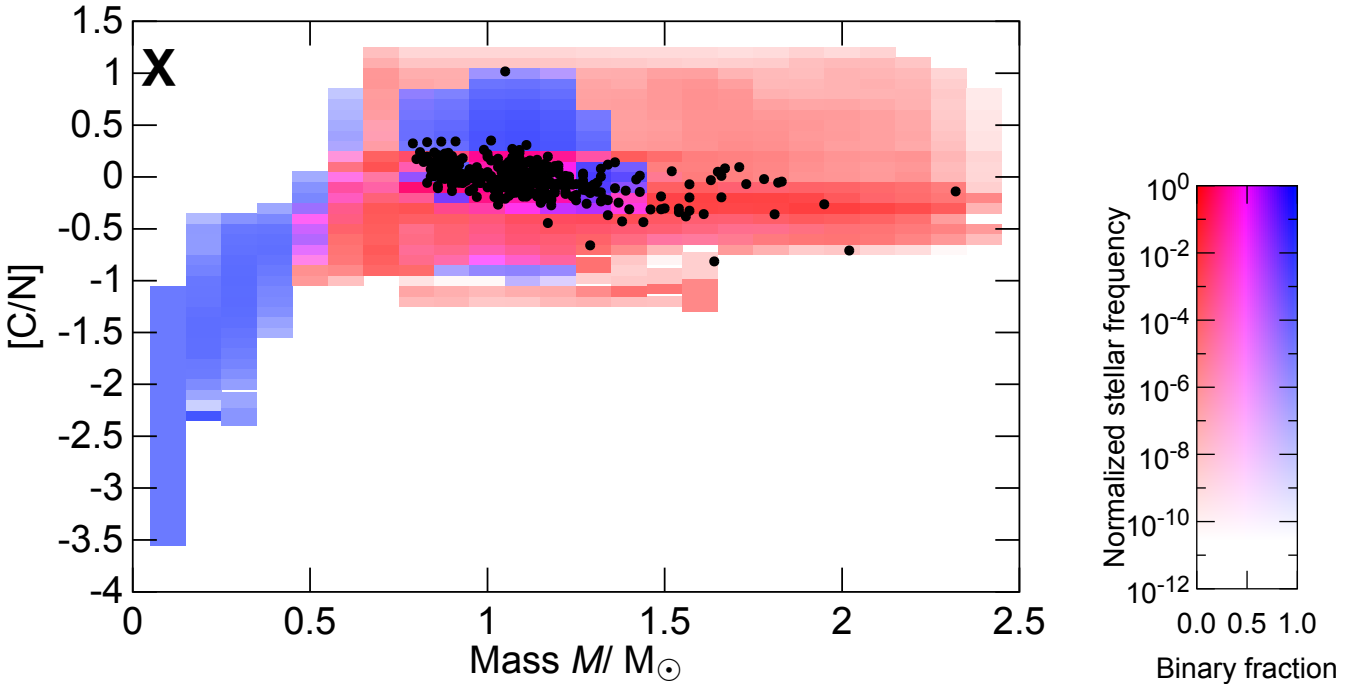


Figure 5. $[C/N]$ vs mass in our model set X, which best represents an unbiased thick-disc stellar population, with the $[C/N]$ range chosen to include all giant stars in our model including stripped giants (Algols), merged giants and mass-transfer products (AGB and CH stars). The depth of shading represents the (logarithm of) the number of stars in each bin relative to the maximum. The colour is the binary fraction: single stars are red while binary stars are blue.

Hoyle wind accretion is not efficient enough to make many stars with $M > 1.3 M_{\odot}$ because typically only about $0.1 M_{\odot}$ accretes (Abate et al. 2013). Only the merging channel makes stars more massive than $1.3 M_{\odot}$ when there is no wind-RLOF and, likewise, only 6.9 per cent of giants more massive than $1.3 M_{\odot}$ are blue stragglers on the main sequence. In our low-metallicity model sets, B2 with $Z = 10^{-3}$ and B3 with $Z = 10^{-4}$, many more carbon-rich stars are made because carbon production in AGB stars is more efficient in low-mass stars at low metallicity (Karakas et al. 2002; Izzard & Tout 2004). Model set B3 has fewer carbon-rich, massive giants because there are few stars with $M > 1.3 M_{\odot}$ that satisfy our age criteria at $Z = 10^{-4}$.

Using our alternative Roche-lobe overflow rate calculation schemes (B11, B12) has little effect. Changing our prescription of angular momentum loss during non-conservative RLOF (B15–18), γ_{RLOF} , has no effect because mass transfer is either conservative, so γ_{RLOF} is irrelevant, or proceeds through common-envelope evolution. Allowing for the companion-reinforced attrition process (CRAP) with $B_C = 10^3$ and 10^4 in model sets B13 and B14 changes the fraction of giant stars in excess of $1.3 M_{\odot}$ to 1.5 per cent and 1.0 per cent respectively. Increasing B_C is the only way, other than increasing the metallicity, to increase the number of binaries among our simulated red giants with $M > 1.3 M_{\odot}$.

One model set stands out from the others in terms of number of giants with $M \gtrsim 1.3 M_{\odot}$. In model set B19 we use the a logarithmically-flat separation distribution (Appendix B2), $dN \propto d \log a$ where a is the orbital separation, rather than the log-normal distribution of Duquennoy & Mayor (1991). This enhances the number of initially close binaries and hence also the number of stars which transfer mass or merge. The fraction of giants with

$M > 1.3 M_{\odot}$ increases to 11 per cent, far closer to the 14 per cent of the APOKASC data. We discuss this further in the following section.

5 DISCUSSION

Our simulated stellar populations match the range of abundances and masses observed in the APOKASC red-giant sample, but a number of uncertainties – in the models, observations and interpretation – remain. Alternative evolutionary pathways, such as triple stars and stellar migration, are possible. We discuss these below and suggest avenues for future research that may help resolve the associated problems.

5.1 Range of $[C/N]$ and mass vs. APOKASC and the number of massive thick-disc stars

Interactions in binary-star systems naturally explain the range of masses in the APOKASC thick-disc sample of red giants, from 0.9 to about $2 M_{\odot}$ and their range in surface $[C/N]$. Many of these binaries are expected to merge and evolve as single giant stars, which also accounts for the low binary frequency among these extra-massive stars. However, the number of stars more massive than $1.3 M_{\odot}$ in the APOKASC thick-disc sample is 14 per cent. It is difficult to reproduce such a large fraction of stars with our stellar population models.

Our model set B19, with a logarithmically-flat orbital separation distribution (Appendix B2), contains enough sufficiently close binary stars that 11 per cent of thick-disc stars are expected to exceed

$1.3 M_{\odot}$, assuming that all stars are born with companions. In the solar neighbourhood about half of $1 M_{\odot}$ stars are binary and a log-normal distribution of periods peaking at many years (Duquennoy & Mayor 1991) is more representative than a logarithmically-flat initial-separation distribution. If such distributions also apply to the thick disc, it is difficult to see how all the 14 per cent of these extra-massive stars can be made in binary systems. Recent suggestions of a high multiplicity fraction, perhaps in excess of two thirds, among old stars also helps reconcile our models and the observational data (Fuhrmann et al. 2017b).

5.2 Extra mixing

Our population nucleosynthesis models do not include mixing except convection and thermohaline mixing of accreted material. They may then not be able to reproduce observed extra mixing near the tip of the red giant branch (Lagarde et al. 2012) nor any nitrogen depletion at the helium flash (Masseron et al. 2017). However, our APOKASC red giant branch stars are not bright enough to have yet undergone canonical extra mixing which should occur near the tip of the red giant branch. So we need not implement extra mixing in our models.

Our APOKASC red clump stars are more problematic. Masseron et al. (2017) show that, at metallicities around 0 and -0.55 , $[N/Fe]$ drops by 0.1 and 0.2 dex at the helium flash, while $[C/Fe]$ decreases by at most 0.1 dex. Most of our thick-disc stars have $0 < [Fe/H] < -0.4$, so a change in $[C/N]$ of about -0.25 dex is possible at the tip of the red giant branch. The scatter in $[C/N]$ among our APOKASC stars more massive than $1.3 M_{\odot}$ is several times this, with $+0.1 \lesssim [C/N] \lesssim -0.8$. So selecting only red giant branch (hydrogen burning) or red clump (helium burning) stars does not change our overall conclusion.

Binary interaction is unlikely to solve the question of extra mixing at helium ignition and associated depletion of nitrogen. This depletion is seen in the bulk of stars, many of which are presumably single, and so not among the few per cent which have exchanged mass or merged. Mass transfer also only increases the likelihood of a deeper first dredge up, more canonical extra mixing and a further increase in nitrogen.

5.3 Binary properties as a function of mass and orbital period

The binary fraction among stars more massive than our threshold mass of $1.3 M_{\odot}$ depends little on most of our model parameters. This reflects the two mechanisms for making stars more massive than $1.3 M_{\odot}$ star in the thick disc. Wind mass accretion, in which the system is and remains binary, only increases the stellar mass by a few tenths of a solar mass at most. In contrast, merging can nearly double the mass of a star and merged binary-star systems are always single. This is clear from Fig. 3 B1a: the blue (binary-star) region extends to around $M = 1.5 M_{\odot}$ but no further, while the red region (single stars only) dominates at high mass. This is a feature typical of all our model sets: the most massive stars have merged and should all be single or have a wide companion if initially in a triple system (Toonen et al. 2016). Our result agrees qualitatively with that of Jofré et al. (2016) who conclude that stars less massive than $1.2 M_{\odot}$ are more likely to be in binaries than those more massive than $1.2 M_{\odot}$. In section 5.4 we discuss changes to the mass threshold.

The bulk of stars in model set B1, with $M = 1.1 M_{\odot}$ and $[C/N] = 0$, have an orbital period distribution which is very similar

to the initial distribution of orbital periods of G/K dwarfs (Fig. 6). Our CH stars, with $M = 1.2 M_{\odot}$ and $[C/N] = 0.5$, have an orbital-period distribution similar to that predicted for barium stars (Izzard et al. 2010). A period gap between 10 and 1000 d, caused by orbital shrinkage during common envelope evolution, is clearly visible (e.g. Pols et al. 2003; Dermine et al. 2013; Vos et al. 2015). The Algol systems are all in short period binaries, as we expect of low-mass giants undergoing Roche-lobe overflow.

Our models predict a small number of short-period binaries equivalent to low-mass Algol systems. Given their low mass these stars may be rejected by APOKASC or may be too dim to be seen in great numbers. Our prediction number of Algols is similar to the 0.1 – 0.2 per cent of Galactic disc stars predicted by Malkov et al. (2017). Interaction is more likely in giant stars than in field dwarfs, which at least partly explains our greater predicted frequency. If the number of Algols can be measured accurately it may allow us to constrain the initial-period distribution. Our lower-metallicity model sets, B2 with $Z = 10^{-3}$ and B3 with $Z = 10^{-4}$, have Algol fractions of 2.6 per cent and 2.8 per cent, suggesting that any observational campaign will have to be careful to select stars by metallicity.

5.4 Thick disc membership: metallicity and age, threshold mass

Our thick-disc selection is probably biased. *Kepler* observed only a small fraction of the sky, so does not sample well the whole thick or thin disc, and the sample is magnitude rather than volume limited. The metallicity distribution in the APOKASC sample (Fig. 2) suggests that a fraction of the stars more massive than $1.3 M_{\odot}$ are actually high-metallicity interlopers whose origin is not in binary-star interaction (Navarro et al. 2011).

Our thick-disc age criteria are likely rather simplistic. We deliberately choose our age range, 5 to 10 Gyr, to match the masses reported by APOKASC, assuming a metallicity of $Z = 0.008$ ($[Fe/H] = -0.24$). The APOKASC masses may be systematically overestimated by 10 – 15 per cent because they are derived from scaling relations rather than more sophisticated techniques (Gaulme et al. 2016; Rodrigues et al. 2017).

To compensate for this, we can select older stars of lower mass, hence greater age, when they are giants, as in our model set B20 with ages 8 to 13 Gyr. The number of stars with mass in excess of $1.3 M_{\odot}$ reduces from 1.7 per cent to 0.81 per cent. However, this test is unfair. We must also reduce our threshold mass to reflect the increase in age. In model set S5, the single-star equivalent of B20, there are no stars of mass exceeding $1.0 M_{\odot}$. The fractions of giant stars with masses exceeding 1.0, 1.1 and $1.2 M_{\odot}$ in model set B20 are 8.91 per cent, 2.32 per cent and 1.02 per cent, respectively.

The best solution to the above problem is to construct a full thick-disc population made up of models with a distribution of metallicity. We shall do this in the future. Here we concentrate on the effects of binary stars.

5.5 Masses and core masses

Our limited statistical analysis avoids the unpleasant task of taking into account the sometimes significant errors on the APOKASC masses. We assume that, in bulk, these errors have little effect on the relatively large fraction (14 per cent) of stars with masses in excess of $1.3 M_{\odot}$. Of 300 stars, and given the high-metallicity interlopers described above, this seems reasonable.

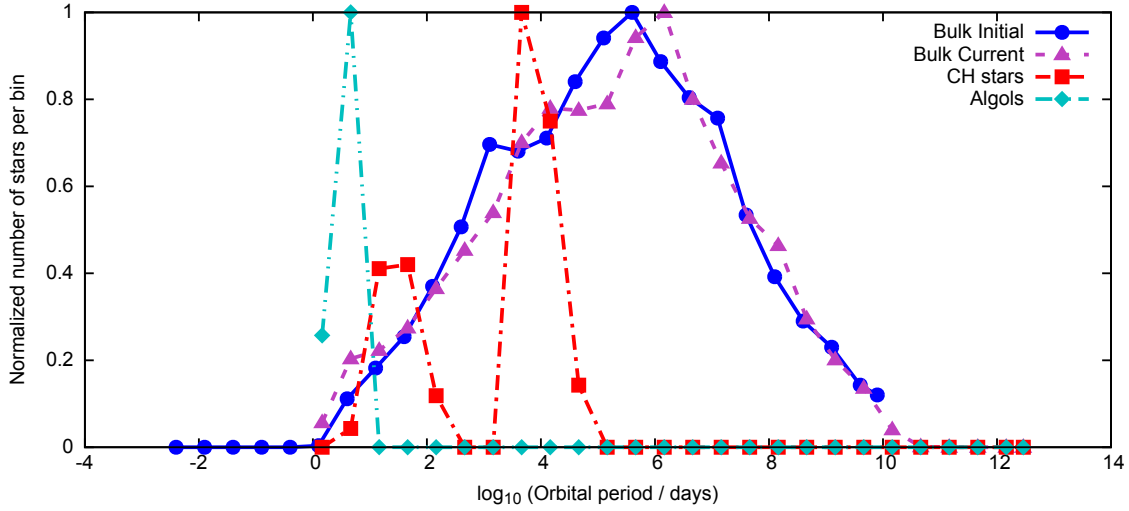


Figure 6. Orbital period distributions in our default model set of thick-disc binary giants, B1. The blue circles and purple triangles show the initial and current distributions among the bulk of our model stars with $M = 1.10 \pm 0.05 M_{\odot}$ and $[C/N] = 0 \pm 0.05$. The red squares show the period distribution of our CH stars with $M = 1.20 \pm 0.05 M_{\odot}$ and $[C/N] = 0.50 \pm 0.05$. The cyan diamonds show the period distribution of the Algol-like systems with $M = 0.20 \pm 0.05 M_{\odot}$ and $[C/N] = -1.50 \pm 0.05$. Logarithmic bins in orbital period are 0.5 dex wide and each distribution has its peak normalized to 1.0. The bulk initial distribution is slightly different to our initial binary period distribution because only some stars enter the range given by $M = 1.10 \pm 0.05 M_{\odot}$ and $[C/N] = 0 \pm 0.05$.

The distributions of masses and core masses of giant stars in our model sets S1, B1, B19 and B21 are shown in Fig. 7. The tail of stars of mass greater than $1.3 M_{\odot}$ is clear in the binary-star model sets (B1, B19 and B21), while it is absent in the single-star model set (S1). The bulk distribution of core masses differs little between single and binary stars. The small fraction of stars more massive than $1.3 M_{\odot}$ contributes to a high-mass tail in both mass and core mass.

Model set B21 is exceptional. In this model set we select stars with $-2 \leq \log_{10}(g/\text{cm}^2\text{s}^{-1}) \leq 3$ to match our APOKASC data selection. This range of $\log g$ contains the red clump (core helium burning) stars which have a core mass of about $0.5 M_{\odot}$ so stars with this core mass are artificially enhanced in number. A good understanding of selection effects is thus critical to matching any core-mass distribution measured, e.g. by asteroseismology, to stellar evolution models. The distribution of stellar masses does not suffer from such a problem because the mass of the red clump stars is only slightly less than that of stars on the red giant branch. This is caused by mass loss at the tip of the giant branch prior to core helium burning (Miglio et al. 2012). The peak of the mass distribution of stars in B21 is thus shifted to slightly lower mass than in S1, B1 or B19.

5.6 Comparison with CEMP-*s* stars

The number of massive thick-disc stars in our models, typically 2 per cent compared to the observed 14 per cent, may suggest that there are young interlopers in the observed sample. However, there is circumstantial evidence from another stellar population that supports significant binary-star mass transfer. The *s*-process rich, carbon-enhanced metal-poor (CEMP-*s*) stars of the Galactic halo have metallicities $[\text{Fe}/\text{H}] \leq -2$ and are found in intermediate-period binary systems (Tsangarides et al. 2004; Lucatello et al. 2005; Starkenburg et al. 2014). Carbon and *s*-process elements are both made in AGB stars. So CEMP-*s* stars probably form by mass transfer from an AGB star similarly to CH and barium stars (Mc-

Clure et al. 1980; McClure 1984; Jorissen 1999). CEMP-*s* stars constitute 10 to 20 per cent of the extremely-metal poor (EMP) population (Lucatello et al. 2006; Lee et al. 2014) while standard binary population synthesis models predict a CEMP/EMP ratio of about 2 per cent at $[\text{Fe}/\text{H}] = -2.3$ (Izzard et al. 2009). The predicted number of CEMP-*s* stars is increased if more are born with short and intermediate orbital periods which are close enough for efficient mass transfer. A logarithmically-flat initial-separation distribution rather than log-normal initial-period distribution does just this (Appendix B). Such an initial distribution of binary periods also increases the number of thick-disc stars with masses exceeding $1.3 M_{\odot}$, as required to match the APOKASC data.

5.7 Alternatives to our binary-star scenario

To increase the number of thick-disc stars with masses in excess of $1.3 M_{\odot}$ without invoking binary interactions, a young, metal-poor, α -rich population is required. It has been suggested that Galactic migration is responsible for populating the thick disc with such stars (Chiappini et al. 2015). We cannot investigate this claim with our models but we know binary stars exist at all metallicities so there should be many in the thick disc. So some will interact and the question is how many. As we discuss above the initial distribution of orbits is key. To make 10 per cent of giants more massive than $1.3 M_{\odot}$ we need a logarithmically-flat initial-separation distribution, so that there are many more interacting low-mass binaries than predicted by the solar neighbourhood orbital period distribution. The CEMP-*s* number problem (Sec. 5.6) also requires an orbital separation distribution with many interacting binaries, so qualitatively supports our use of this distribution even if the evidence is rather circumstantial. It is possible that triple-star interactions lead to a similar number of interacting binaries even with an initial orbital period distribution more like that of the solar neighbourhood. However quantitative predictions are still rather preliminary (Toonen et al. 2016).

The migration scenario cannot solve the CEMP-*s* number prob-

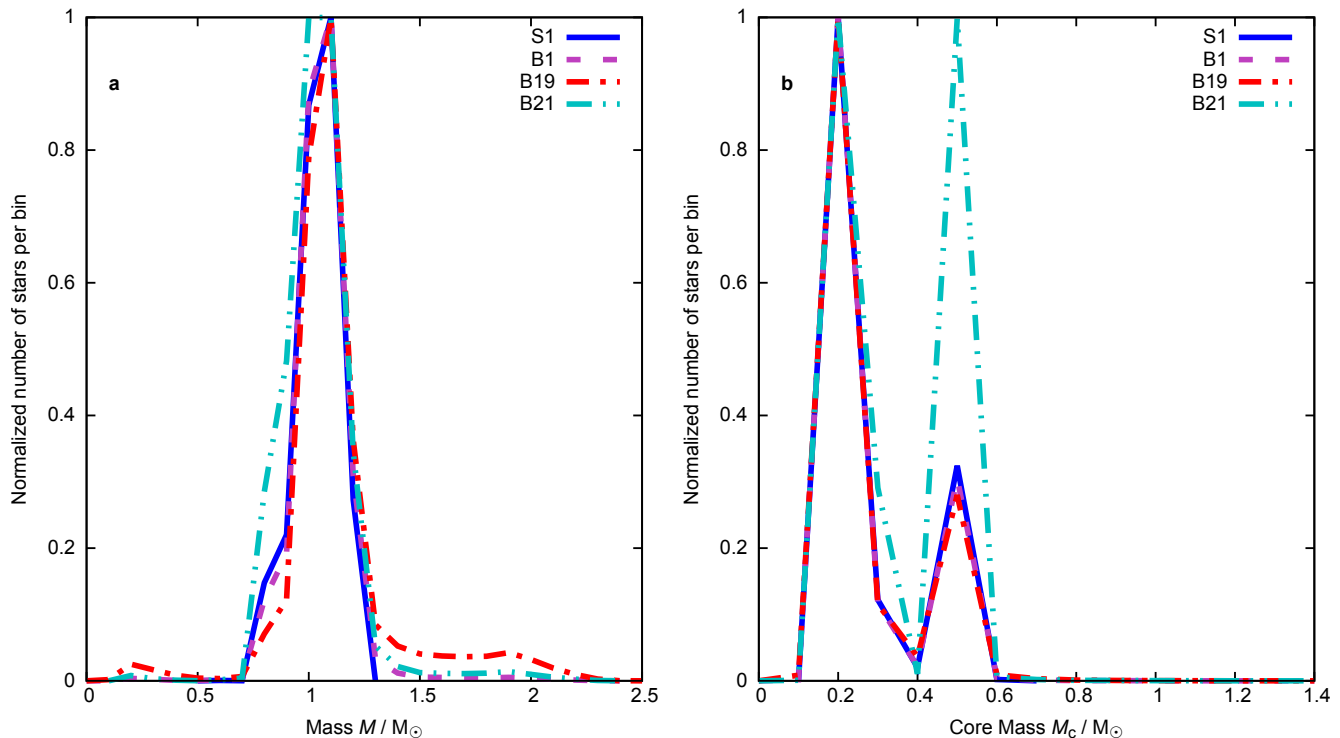


Figure 7. Mass (panel **a**, left) and core mass (panel **b**, right) distributions in our model sets S1 (single stars with default physics), B1 (initially-binary stars only with default physics), B19 (as B1 with a logarithmically-flat initial-separation distribution) and B21 (as B1 with $2 \leq \log_{10}(g/\text{cm}^2\text{s}^{-1}) \leq 3$ selection to mimic the APOKASC data). Bins have a fixed width of $0.1 M_{\odot}$ and the peak of each distribution is normalized to 1.0. The tail of stars more massive than $1.3 M_{\odot}$ is clear in panel **a** and a tail of fewer stars with core mass in excess of $0.6 M_{\odot}$ can be seen in panel **b**.

lem either. First these stars are found in the Galactic halo, which is likely to undergo migration on far longer spatial or temporal scales than the thick disc. Could enough carbon-rich stars be formed and migrate into the, especially outer (Carollo et al. 2012), halo in 14 Gyr? Secondly, if CEMP-*s* stars are young and single, as in the migration scenario, they are born with $[C/Fe] > +1$ and metallicity $[Fe/H] \lesssim -2$. Recent star formation under such conditions in our Galaxy is unknown. Occam’s razor therefore favours that interaction in intermediate-period binaries, which are well known to exist, as an explanation for CEMP-*s* stars.

We have shown that thick-disc stars more massive than $1.3 M_{\odot}$ can be formed in interacting binaries or higher order multiple stellar systems. We have good reason to think such systems exist but there may well be some contribution to the massive thick-disc population from migration of younger stars. Differentiation between the two possibilities may be possible when we better know the binary fraction and orbital period distribution of the stars more massive than $1.3 M_{\odot}$. Our simulations predict that many of these stars are merged, hence single. They may also be wide binaries which were triples. The migration scenario would predict a binary fraction and orbital period distribution which are similar to those of the stars at birth.

5.8 Blue stragglers

Many of our modelled thick-disc stars with masses greater than $1.3 M_{\odot}$ accrete mass while they are on the main sequence. They thus pass through a blue-straggler phase during which they look younger than the main-sequence lifetime corresponding to their mass. This simple definition of a blue straggler quietly neglects the many selection effects which plague quantitative attempts to count such systems (Geller et al. 2013 and the discussion of Schneider et al. 2014 and references therein). In most of our model sets, 10 to 30 per cent of giants more massive than $1.3 M_{\odot}$ are expected to be blue stragglers before they ascend the giant branch. Most of these form by wind mass transfer and hence some are expected to be enhanced in carbon and *s*-process elements. If wind-RLOF is disabled, as in model set B9, the number of giants that were blue stragglers drops from the 16 per cent of model set B1 to just 6.9 per cent. If the relative number and chemical properties of blue stragglers in the thick disc can be assessed, perhaps by barium abundance to detect pollution from a TPAGB donor, the effect of wind-RLOF may be quantifiable. A first attempt suggests around 10 per cent of thick-disc main-sequence stars may be blue stragglers (Fuhrmann et al. 2017a). Four of the APOKASC stars more massive than $1.3 M_{\odot}$ are, however, not rich in barium (Yong et al. 2016) suggesting they are post-main sequence mergers.

5.9 Model uncertainties: binary physics, nucleosynthesis

While our input distributions are rather uncertain, our binary star model suffers from uncertainty too. As discussed above, wind-RLOF is required to make a significant number of binary-star giants with masses in excess of $1.3 M_{\odot}$. We also test our prescriptions for common-envelope evolution, companion-reinforced attrition and mass transfer. Changing the appropriate parameters in our model has limited effect on our results, certainly less than changing the initial-period distribution.

Our nucleosynthesis model, while an improvement on previous versions of `BINARY_C`, is still far from perfect even if it well reproduces single-star evolution. We assume that stars undergo first dredge up to a depth the time dependence of which is calculated by the `BSE` algorithm (Hurley et al. 2000, 2002) and limited to a maximum depth given by our `STARS` models.

For evolved stars on the red giant branch, the entire convective envelope is mixed to a depth $M_{\text{env}} = M - M_{\text{c}}$. This is fitted to the mass M_0 which is defined by Hurley et al. (2000) as the mass of the star at the base of the giant branch that goes on to determine its core mass. This is the same approach taken in `BSE` to calculate the stellar evolution of red giant stars but it neglects the fact that the core mass to mass ratio, M_{c}/M , is different to that of a single star of the same total mass. The effect of a variable, off-grid, M_{c}/M on the depth of first dredge up in such stars remains to be tested with detailed stellar models.

We further assume that common-envelope evolution mixes the stellar envelope right down to the core (Ivanova 2011). This may be deeper than the convective envelope has mixed at that phase of evolution, particularly if common-envelope evolution occurs early on the giant branch. Given the energy injected into the envelope by orbital decay of the companion star which itself likely descends to near the core-envelope boundary, this seems reasonable. Unfortunately, existing stellar evolution models of common-envelope evolution, and especially stars that merge during this phase, do not go on to predict the subsequent evolution of the stars except in a few cases (e.g. Zhang & Jeffery 2013; Vos et al. 2015). This issue should be addressed in the future.

6 CONCLUSIONS

We explore the properties of the binary-star population of low-mass stars in the thick disc which are more massive than they should be given their age. Our models naturally contain a population of red giant stars, from 1 to 10 per cent of all giants, more massive than the maximum $1.3 M_{\odot}$ that is possible in single-star evolution. These stars are more likely to be single, merged objects than binary stars, even when common-envelope ejection is efficient ($\alpha_{\text{CE}} = 1$). Some may be wide binaries that were originally hierarchical triple systems. Modelling uncertainties are generally not important, except that wind Roche lobe overflow or companion-reinforced attrition are required to make binary stars with $M > 1.3 M_{\odot}$, and that to make as many as seen in APOKASC we require a logarithmically-flat initial orbital period distribution with many initially close binary stars. Single-stars made by merging processes likely have a peculiar mass to core-mass ratio which could be measured asteroseismologically by targeting the most massive stars in APOKASC or similar samples. It is also crucial to comprehensively monitor the radial velocities of the thick-disc stars which are anomalously massive, such as those found in APOKASC, to know their orbital periods and binary fraction. This work continues in parallel to our theoretical study.

ACKNOWLEDGEMENTS

We thank the referee for their suggestions which have improved the clarity of the manuscript. RGI thanks the STFC for funding his Rutherford fellowship under grant ST/L003910/1, Churchill College, Cambridge for his fellowship and access to their library, and Carlo Abate, Guy Davies, Ilya Mandel, Andrea Miglio and Richard Stancliffe for useful discussions. RGI and GMH thank the STFC for funding Rutherford grant ST/M003892/1. HPP thanks the STFC for funding her research studentship. PJ and TM acknowledge support from the European Union FP7 programme through ERC grant number 320360. TM acknowledges support provided by the Spanish Ministry of Economy and Competitiveness (MINECO) under grant AYA-2014-58082-P and AYA2014-56359-P. CAT thanks Churchill College, Cambridge for his fellowship. This research has made use of NASA's Astrophysics Data System Bibliographic Services. We thank Dave Green for his Cubehelix colour scheme (Green 2011) and his debugging of *MNRAS*' new class file.

References

- Abate C., Pols O. R., Izzard R. G., Mohamed S. S., de Mink S. E., 2013, *A&A*, **552**, A26
- Abate C., Pols O. R., Stancliffe R. J., Izzard R. G., Karakas A. I., Beers T. C., Lee Y. S., 2015, *A&A*, **581**, A62
- Adamczak J., Lambert D. L., 2013, *ApJ*, **765**, 155
- Anders E., Grevesse N., 1989, *Geochimica et Cosmochimica Acta*, **53**, 197
- Asplund M., Grevesse N., Sauval A. J., Scott P., 2009, *ARA&A*, **47**, 481
- Bensby T., Feltzing S., 2006, *MNRAS*, **367**, 1181
- Bland-Hawthorn J., Gerhard O., 2016, *ARA&A*, **54**, 529
- Bondi H., Hoyle F., 1944, *MNRAS*, **104**, 273
- Brogaard K., et al., 2016, *Astronomische Nachrichten*, **337**, 793
- Brook C. B., et al., 2012, *MNRAS*, **426**, 690
- Carollo D., et al., 2012, *ApJ*, **744**, 195
- Charbonnel C., Lagarde N., 2010, *A&A*, **522**, A10
- Chiappini C., et al., 2015, *A&A*, **576**, L12
- Claeys J. S. W., Pols O. R., Izzard R. G., Vink J., Verbunt F. W. M., 2014, *A&A*, **563**, A83
- Davies G. R., Miglio A., 2016, *Astronomische Nachrichten*, **337**, 774
- De Marco O., Izzard R. G., 2017, *Publ. Astron. Soc. Australia*, **34**, e001
- Denissenkov P. A., Pinsonneault M., 2008, *ApJ*, **679**, 1541
- Dermine T., Izzard R. G., Jorissen A., Van Winckel H., 2013, *A&A*, **551**, A50
- Dewi J. D. M., Tauris T. M., 2000, *A&A*, **360**, 1043
- Duquenois A., Mayor M., 1991, *A&A*, **248**, 485
- Eggleton P. P., 1971, *MNRAS*, **151**, 351
- Eldridge J. J., Tout C. A., 2004, *MNRAS*, **348**, 201
- Elsworth Y., Hekker S., Basu S., Davies G. R., 2017, *MNRAS*, **466**, 3344
- Feltzing S., Bensby T., 2009, in Mamajek E. E., Soderblom D. R., Wyse R. F. G., eds, *IAU Symposium Vol. 258, The Ages of Stars*. pp 23–30 ([arXiv:0811.2445](https://arxiv.org/abs/0811.2445)), doi:10.1017/S1743921309031676
- Fuhrmann K., Chini R., Kaderhandt L., Chen Z., 2017a, *MNRAS*, **464**, 2610
- Fuhrmann K., Chini R., Kaderhandt L., Chen Z., 2017b, *ApJ*, **836**, 139
- Gaburov E., Lombardi J. C., Portegies Zwart S., 2008, *MNRAS*, **383**, L5
- Gaulme P., et al., 2016, *ApJ*, **832**, 121
- Geller A. M., Mathieu R. D., 2011, *Nature*, **478**, 356
- Geller A. M., Hurley J. R., Mathieu R. D., 2013, *AJ*, **145**, 8
- Gilmore G., Reid N., 1983, *MNRAS*, **202**, 1025
- Green D. A., 2011, *Bulletin of the Astronomical Society of India*, **39**, 289
- Haywood M., Di Matteo P., Lehnert M. D., Katz D., Gómez A., 2013, *A&A*, **560**, A109
- Holtzman J. A., et al., 2015, *AJ*, **150**, 148
- Hurley J. R., Pols O. R., Tout C. A., 2000, *MNRAS*, **315**, 543
- Hurley J. R., Tout C. A., Aarseth S. J., Pols O. R., 2001, *MNRAS*, **323**, 630
- Hurley J. R., Tout C. A., Pols O. R., 2002, *MNRAS*, **329**, 897
- Hut P., 1981, *Astronomy and Astrophysics*, **99**, 126

- Ivanova N., 2011, *ApJ*, **730**, 76
- Ivanova N., et al., 2013, *A&Arv*, **21**, 59
- Izzard R. G., Tout C. A., 2004, *MNRAS*, **350**, L1
- Izzard R. G., Tout C. A., Karakas A. I., Pols O. R., 2004, *MNRAS*, **350**, 407
- Izzard R. G., Dray L. M., Karakas A. I., Lugaro M., Tout C. A., 2006, *A&A*, **460**, 565
- Izzard R. G., Glebbeek E., Stancliffe R. J., Pols O. R., 2009, *A&A*, **508**, 1359
- Izzard R. G., Dermine T., Church R. P., 2010, *A&A*, **523**, A10
- Izzard R. G., Hall P. D., Tauris T. M., Tout C. A., 2012, in *Proceedings of IAU Symposium 283*, pp 95–102, doi:10.1017/S1743921312010769
- Jofré P., et al., 2016, *A&A*, **595**, A60
- Jorissen A., 1999, in *IAU Symp. 191: Asymptotic Giant Branch Stars*, eds. T. Le Bertre, A. Lebre, and C. Waelkens. p. 437
- Jorissen A., Van Eck S., Mayor M., Udry S., 1998, *A&A*, **332**, 877
- Karakas A. I., Lattanzio J. C., Pols O. R., 2002, *Publ. Astron. Soc. Australia*, **19**, 515
- Kroupa P., Tout C., Gilmore G., 1993, *MNRAS*, **262**, 545
- Kudritzki R., Reimers D., 1978, *Astronomy and Astrophysics*, **70**, 227
- Lagarde N., Decressin T., Charbonnel C., Eggenberger P., Ekström S., Palacios A., 2012, *A&A*, **543**, A108
- Lee Y. S., Suda T., Beers T. C., Stancliffe R. J., 2014, *ApJ*, **788**, 131
- Lodders K., 2010, *Astrophysics and Space Science Proceedings*, **16**, 379
- Lombardi Jr. J. C., Warren J. S., Rasio F. A., Sills A., Warren A. R., 2002, *ApJ*, **568**, 939
- Lucatello S., Tsangarides S., Beers T. C., Carretta E., Gratton R. G., Ryan S. G., 2005, *ApJ*, **625**, 825
- Lucatello S., Beers T. C., Christlieb N., Barklem P. S., Rossi S., Marsteller B., Sivarani T., Lee Y. S., 2006, *ApJ*, **652**, L37
- Malkov O. Y., Kovaleva D. A., Yungelson L. R., Avvakumova E. A., Chulkov D. A., Dluzhnevskaya O. B., Kniazev A. Y., 2017, *Baltic Astronomy*, **25**, 384
- Martig M., Minchev I., Ness M., Fousneau M., Rix H.-W., 2016, *ApJ*, **831**, 139
- Masseron T., Gilmore G., 2015, *MNRAS*, **453**, 1855
- Masseron T., Lagarde N., Miglio A., Elsworth Y., Gilmore G., 2017, *MNRAS*, **464**, 3021
- Matrozis E., Stancliffe R. J., 2016, *A&A*, **592**, A29
- Matrozis E., Stancliffe R. J., 2017, *A&A* (in press), arXiv 1707.09434,
- McClure R. D., 1984, *ApJ*, **280**, L31
- McClure R. D., Fletcher J. M., Nemeč J. M., 1980, *ApJ*, **238**, L35
- Miglio A., et al., 2012, *MNRAS*, **419**, 2077
- Miglio A., et al., 2016, *MNRAS*, **461**, 760
- Minchev I., Steinmetz M., Chiappini C., Martig M., Anders F., Matijevic G., de Jong R. S., 2017, *ApJ*, **834**, 27
- Moe M., Di Stefano R., 2017, *ApJS*, **230**, 15
- Mohamed S., Podsiadlowski P., 2007, in R. Napiwotzki & M. R. Burleigh ed., *Astronomical Society of the Pacific Conference Series Vol. 372*, 15th European Workshop on White Dwarfs. p. 397
- Navarro J. F., Abadi M. G., Venn K. A., Freeman K. C., Anguiano B., 2011, *MNRAS*, **412**, 1203
- Nieuwenhuijzen H., de Jager C., 1990, *A&A*, **231**, 134
- Öpik E., 1924, *Publications of the Tartu Astrofizika Observatory*, **25**
- Palacios A., Jasniewicz G., Masseron T., Thévenin F., Itam-Pasquet J., Parthasarathy M., 2016, *A&A*, **587**, A42
- Pinsonneault M. H., et al., 2014, *ApJS*, **215**, 19
- Pols O. R., Tout C. A., Eggleton P. P., Han Z., 1995, *MNRAS*, **274**, 964
- Pols O. R., Karakas A. I., Lattanzio J. C., Tout C. A., 2003, in *Corradi R. L. M., Mikolajewska J., Mahoney T. J.*, eds, *Astronomical Society of the Pacific Conference Series Vol. 303*, *Astronomical Society of the Pacific Conference Series*. p. 290
- Raghavan D., et al., 2010, *ApJS*, **190**, 1
- Rodrigues T. S., et al., 2017, *MNRAS*,
- Salaris M., Pietrinferni A., Piersimoni A. M., Cassisi S., 2015, *A&A*, **583**, A87
- Sana H., et al., 2012, *Science*, **337**, 444
- Sandage A. R., 1953, *AJ*, **58**, 61
- Sandage A. R., Schwarzschild M., 1952, *ApJ*, **116**, 463
- Schneider F. R. N., et al., 2014, *ApJ*, **780**, 117
- Schröder K.-P., Pols O. R., Eggleton P. P., 1997, *MNRAS*, **285**, 696
- Siess L., Izzard R. G., Davis P. J., Deschamps R., 2013, *A&A*, **550**, A100
- Sills A., Glebbeek E., 2010, *MNRAS*, **407**, 277
- Stancliffe R. J., Eldridge J. J., 2009, *MNRAS*, **396**, 1699
- Stancliffe R. J., Glebbeek E., Izzard R. G., Pols O. R., 2007, *A&A*, **464**, L57
- Stancliffe R. J., Church R. P., Angelou G. C., Lattanzio J. C., 2009, *MNRAS*, **396**, 2313
- Starkenburger E., Shetrone M. D., McConnachie A. W., Venn K. A., 2014, *MNRAS*, **441**, 1217
- Toonen S., Hamers A., Portegies Zwart S., 2016, *Computational Astrophysics and Cosmology*, **3**
- Tout C. A., Eggleton P. P., 1988, *MNRAS*, **231**, 823
- Tout C. A., Aarseth S. J., Pols O. R., Eggleton P. P., 1997, *MNRAS*, **291**, 732
- Tsangarides S., Ryan S. G., Beers T. C., 2004, *MmSAI*, **75**, 772
- Vassiliadis E., Wood P. R., 1993, *ApJ*, **413**, 641
- Vos J., Østensen R. H., Marchant P., Van Winckel H., 2015, *A&A*, **579**, A49
- Weiss A., Denissenkov P. A., Charbonnel C., 2000, *A&A*, **356**, 181
- Wellstein S., Langer N., Braun H., 2001, *A&A*, **369**, 939
- Yong D., et al., 2016, *MNRAS*, **459**, 487
- Yuan H., Liu X., Xiang M., Huang Y., Chen B., Wu Y., Hou Y., Zhang Y., 2015, *ApJ*, **799**, 135
- Zahn J.-P., 1977, *A&A*, **57**, 383
- Zhang X., Jeffery C. S., 2013, *MNRAS*, **p. 656**
- de Mink S. E., Langer N., Izzard R. G., Sana H., de Koter A., 2013, *ApJ*, **764**, 166

APPENDIX A: STELLAR WINDS

In `BINARY_C` we mostly use the stellar wind mass loss prescription of SSE (Hurley et al. 2000). During giant-branch and subsequent evolution a mass-loss rate, \dot{M}_R , is calculated with the formula of Kudritzki & Reimers (1978),

$$\dot{M}_R = \eta 4 \times 10^{-13} \frac{(L/L_\odot)(R/R_\odot)}{(M/M_\odot)} M_\odot \text{ yr}^{-1}, \quad (\text{A1})$$

where $\eta = 0.5$ and M , L and R are the stellar mass, luminosity and radius.

On the early asymptotic giant branch (EAGB) we use the formula of Vassiliadis & Wood (1993),

$$\dot{M}_{\text{VW}}(\mathcal{A}) = 10^{\Gamma(\mathcal{A})} M_\odot \text{ yr}^{-1}, \quad (\text{A2})$$

where

$$\Gamma(\mathcal{A}) = \left[P_{\text{Mira}}/d - 100 \mathcal{A} \max\left(\frac{M}{M_\odot} - 2.5, 0\right) \right] \times 0.0125 - 11.4, \quad (\text{A3})$$

and the Mira pulsation period P_{Mira} is,

The EAGB superwind mass-loss rate is,

$$\dot{M}_{\text{superwind,EAGB}} = 1.36 \times 10^{-9} \left(\frac{L}{L_\odot}\right) M_\odot \text{ yr}^{-1}. \quad (\text{A4})$$

The wind mass loss rate is then,

$$\dot{M}_{\text{EAGB}} = \min[\dot{M}_{\text{superwind,EAGB}}, \dot{M}_{\text{VW}}(\mathcal{A} = 1)], \quad (\text{A5})$$

as used by (Hurley et al. 2002).

On the thermally-pulsing asymptotic giant branch (TPAGB) we modify the Vassiliadis & Wood (1993) formula according to Karakas et al. (2002) to calculate the wind mass-loss rate,

$$\dot{M}_{\text{TPAGB}} = \min[\dot{M}_{\text{superwind,TPAGB}}, \dot{M}_{\text{VW}}(\mathcal{A} = 0)], \quad (\text{A6})$$

where

$$\dot{M}_{\text{superwind,TPAGB}} = \begin{cases} 0, & P_{\text{Mira}} < 500 \text{ d}, \\ \frac{cL}{v_w L_\odot} & P_{\text{Mira}} \geq 500 \text{ d}, \end{cases} \quad (\text{A7})$$

c is the speed of light in a vacuum and

$$v_w = \min[15.0, \max(-13.5 + 0.056 P_{\text{Mira}}/d, 0)] \text{ km s}^{-1} \quad (\text{A8})$$

is the wind velocity at infinity (Abate et al. 2013). The wind mass-loss rate on the asymptotic giant branch \dot{M}_{AGB} is then \dot{M}_{EAGB} during the EAGB and \dot{M}_{TPAGB} during the TPAGB.

The wind of Nieuwenhuijzen & de Jager (1990) is calculated by

$$\dot{M}_{\text{NJ}} = 9.6 \times 10^{-15} \times \left(\frac{Z}{0.02}\right)^{0.5} \left(\frac{R}{R_\odot}\right)^{0.81} \left(\frac{L}{L_\odot}\right)^{1.24} \left(\frac{M}{M_\odot}\right)^{0.16} M_\odot \text{ yr}^{-1}, \quad (\text{A9})$$

where Z is the metallicity. A Wolf-Rayet mass-loss rate, suitable for stars with thin envelopes, is given by

$$\dot{M}_{\text{WR}} = 10^{-13} \left(\frac{L}{L_\odot}\right)^{1.5} \max(0, 1 - \mu) M_\odot \text{ yr}^{-1}, \quad (\text{A10})$$

where

$$\mu = \begin{cases} \left(1 - \frac{M_c}{M}\right) \min\left\{5, \max\left[1.2, \left(\frac{10^{-4} L}{7L_\odot}\right)^{-0.5}\right]\right\}, & \text{H-giants,} \\ 5(1 - M_c/\min[1.45M - 0.31M_\odot, M]), & \text{He-giants,} \end{cases} \quad (\text{A11})$$

and M_c is the stellar core mass. The luminous blue variable (LBV) mass-loss rate is given by,

$$\dot{M}_{\text{LBV}} = 0.1x^3 \left(\frac{L}{L_{\text{LBV}}} - 1\right) M_\odot \text{ yr}^{-1}, \quad (\text{A12})$$

if $x \equiv 10^{-5}(R/R_\odot)(L/L_\odot)^{-0.5} - 1 > 0$, $L > L_{\text{LBV}} = 6 \times 10^5 L_\odot$ and the star has left the main sequence. $\dot{M}_{\text{LBV}} = 0$ otherwise.

The total wind mass loss rate is then, for nuclear-burning stars,

$$\dot{M}_{\text{wind}} = \max(\dot{M}_R, \dot{M}_{\text{AGB}}, \dot{M}_{\text{NJ}}, \dot{M}_{\text{WR}}) + \dot{M}_{\text{LBV}}, \quad (\text{A13})$$

and zero for stellar remnants (white dwarfs, neutron stars and black holes).

APPENDIX B: INITIAL ORBITAL PERIOD AND SEPARATION DISTRIBUTIONS

In this paper we use either a hybrid initial-period distribution which is a function of initial primary mass, described in section B1, or a logarithmically-flat initial-separation distribution as described in section B2.

B1 Hybrid period distribution

The initial orbital period P distribution is calculated as a function primary mass M_1 and $\mathcal{P} = \log_{10}(P/d)$ where $\max(\mathcal{P}_{\text{min}}, -1) \leq \mathcal{P} \leq 10$. $\mathcal{P}_{\text{min}}(M_1, M_2, Z)$ is the shortest orbital period for which Roche-lobe overflow does not occur at the zero-age main sequence. We obtain this from `BINARY_C`. We define the density function of the probability, p , of finding a binary system with the logarithm of its orbital period between \mathcal{P} and $\mathcal{P} + d\mathcal{P}$ given it has primary mass M_1 by,

$$\psi = \psi(M_1, \mathcal{P}) = \frac{dp}{d\mathcal{P}} = \mathcal{H} \mathcal{G} \left\{ \exp\left[-\frac{(\mathcal{P} - \mu)^2}{2\sigma^2}\right] + \frac{\mathcal{K}}{\max(0.1, \mathcal{P})} \right\}, \quad (\text{B1})$$

where

$$\mathcal{M} = \max[1.15, \min(16.3, M_1/M_\odot)], \quad (\text{B2})$$

$$f(\mathcal{M}, b, a) = a + (b - a) \left(\frac{\mathcal{M} - 1.15}{16.3 - 1.15}\right), \quad (\text{B3})$$

$$\mu = \mu(\mathcal{M}) = f(\mathcal{M}, -17.8, 5.03), \quad (\text{B4})$$

$$\sigma = \sigma(\mathcal{M}) = f(\mathcal{M}, 9.18, 2.28), \quad (\text{B5})$$

$$\mathcal{K} = \mathcal{K}(\mathcal{M}) = f(\mathcal{M}, 0.0693, 0), \quad (\text{B6})$$

$$\mathcal{G} = \mathcal{G}(\mathcal{M}) = \left(1 + \epsilon^{P-\nu}\right)^{-1}, \quad (\text{B7})$$

$$\nu = \nu(\mathcal{M}) = f(\mathcal{M}, 0.3, -1), \quad (\text{B8})$$

$$\log_{10} \epsilon = -30, \quad (\text{B9})$$

and $\mathcal{H} = \mathcal{H}(\mathcal{M})$ is a normalization factor such that,

$$\mathcal{H}(\mathcal{M}) = \int_{\max(\mathcal{P}_{\text{min}}, -1)}^{10} \psi(\mathcal{M}, \mathcal{P}) d\mathcal{P} = 1. \quad (\text{B10})$$

Fig. B1 shows how Eq. (B1) compares to the power-law distribution, $\psi(\mathcal{P}) \propto \mathcal{P}^{-0.55}$, of Sana et al. (2012) at high mass ($M_1 \geq 16.3 M_\odot$) and the log-normal distribution of Duquennoy & Mayor (1991) at low mass ($M_1 \leq 1.15 M_\odot$). To produce Fig. B1 we assume $\mathcal{P}_{\min}(M_1, M_2, Z) = -1$ because with $M = 1 M_\odot$, $M_2 = 0.5 M_\odot$ and $Z = 0.008$, $\mathcal{P}_{\min} = -0.55$, while with $M_1 = 16 M_\odot$, $M_2 = 8 M_\odot$ and $Z = 0.008$, $\mathcal{P}_{\min} = -0.094$. The observations of Sana et al. (2012) are limited to $\log_{10}(P/d) < 3$. Fig. B2 compares our distribution to that of Moe & Di Stefano (2017, their equation 23) with $M = 1$ and $16 M_\odot$.

B2 Logarithmically-flat initial-separation distribution

Our logarithmically-flat initial-separation distribution is based on that of Öpik (1924) and has been used in many binary population synthesis studies (e.g. Hurley et al. 2002). In the range of initial separations $3 \leq a/R_\odot \leq 10^4$ the probability (p) density function is a flat function of $\log_{10}(a/R_\odot)$,

$$\frac{dp}{d \log_{10}(a/R_\odot)} = \text{constant} = 4 - \log_{10} 3, \quad (\text{B11})$$

and zero otherwise.

APPENDIX C: ORBITAL INCLINATION

Define i , the orbital inclination, to be the angle between the line-of-sight and the normal to the orbital plane of the binary system. Binaries with $i = 0$ and $\pi/2$ are face on and edge on, respectively. The probability that i lies between i and $i + di$, assuming all angles are equally likely, is then

$$P(i) di = \sin i di. \quad (\text{C1})$$

The projected radial velocity is,

$$v = K \sin i, \quad (\text{C2})$$

where $K = K_j$ is the radial velocity semi-amplitude of star $j = 1, 2$,

$$K_j = M_{3-j} \sqrt{\frac{G}{a(1-e^2)(M_1 + M_2)}},$$

where a is the semi-major axis of the orbit, e is the orbital eccentricity and G is Newton's gravitational constant.

If systems with $v > v_{\text{crit}}$ are observed as binary, while systems with $v < v_{\text{crit}}$ are observed as single, the probability that a system with radial velocity amplitude K is observed as a binary is,

$$P(K) = \int_a^b P(i) di, \quad (\text{C3})$$

where $a = \arcsin(v_{\text{crit}}/K)$ and $b = \pi/2$. The probability that a binary system with radial velocity amplitude K is observed as a binary is thus,

$$P(K) = \cos \left[\arcsin \left(\frac{v_{\text{crit}}}{K} \right) \right]. \quad (\text{C4})$$

We set $v_{\text{crit}} = 1 \text{ km s}^{-1}$ in all our model sets.

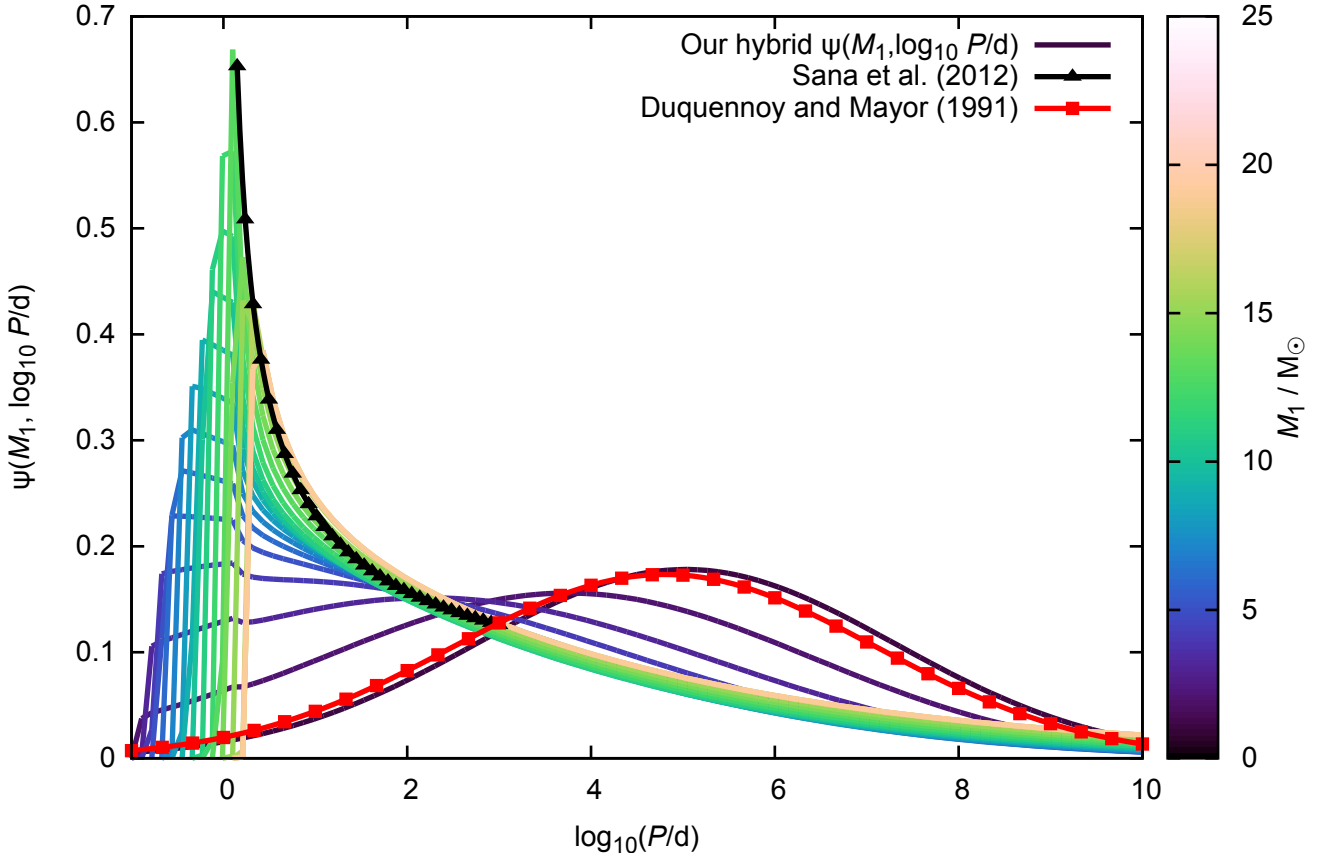


Figure B1. Comparison of our hybrid initial-period distribution, $\psi[M_1, \log_{10}(P/d)]$ of Eq. (B1), as a function of primary-star mass, M_1 , and logarithm of the orbital period, $\log_{10}(P/d)$, to the power-law distribution of Sana et al. (2012, black triangles) at high mass and the log-normal distribution of Duquennoy & Mayor (1991, red squares) at low mass. The curves span the primary mass range 1 to $20 M_{\odot}$ in $1 M_{\odot}$ increments. When we simulate a stellar population orbital periods short enough that Roche-lobe overflow occurs on the main sequence have zero probability even though they are shown in this figure. The short period limit is a function of both stellar masses and metallicity. Note that the observations of Sana et al. (2012) are limited to periods shorter than 1000 d. At longer periods we extrapolate our Eq. (B1).

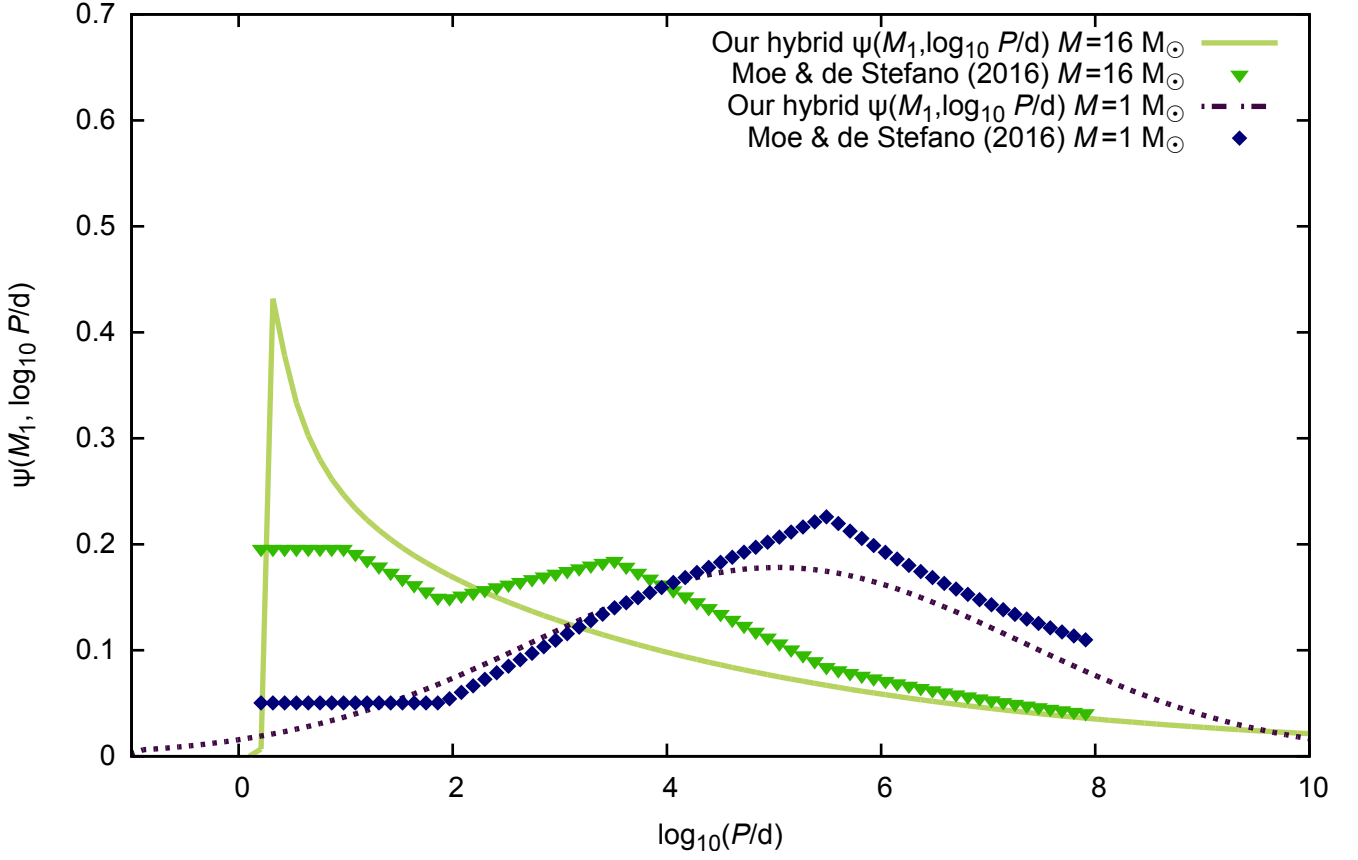


Figure B2. As Fig. B1 at $M = 1$ (blue, dot-dashed line) and $16 M_{\odot}$ (green solid line) compared to the distribution of Moe & Di Stefano (2017) at $M = 1 M_{\odot}$ (blue diamonds) and $M = 16 M_{\odot}$ (green triangles).